

NBI-921352, a first-in-class, Na_v1.6 selective, sodium channel inhibitor that prevents seizures in *Scn8a* gain-of-function mice, and wild-type mice and rats

JP Johnson^{1*}, Thilo Focken², Kuldip Khakh¹, Parisa Karimi Tari³, Celine Dube³, Samuel J Goodchild¹, Jean-Christophe Andrez², Girish Bankar³, David Bogucki^{2,4}, Kristen Burford², Elaine Chang¹, Sultan Chowdhury², Richard Dean¹, Gina de Boer⁴, Shannon Decker², Christoph Dehnhardt², Mandy Feng¹, Wei Gong², Michael Grimwood², Abid Hasan², Angela Hussainkhel¹, Qi Jia², Stephanie Lee⁴, Jenny Li¹, Sophia Lin¹, Andrea Lindgren⁴, Verner Lofstrand², Janette Mezeyova¹, Rostam Namdari⁵, Karen Nelkenbrecher³, Noah Gregory Shuart¹, Luis Sojo⁴, Shaoyi Sun², Matthew Taron², Matthew Waldbrook³, Diana Weeratunge¹, Steven Wesolowski², Aaron Williams¹, Michael Wilson², Zhiwei Xie¹, Rhena Yoo¹, Clint Young¹, Alla Zenova², Wei Zhang², Alison J Cutts⁶, Robin P Sherrington⁷, Simon N Pimstone⁷, Raymond Winquist⁷, Charles J Cohen⁷, James R Empfield⁷

¹In Vitro Biology, Xenon Pharmaceuticals Inc, Burnaby, Canada; ²Chemistry, Xenon Pharmaceuticals Inc, Burnaby, Canada; ³In Vivo Biology, Xenon Pharmaceuticals Inc, Burnaby, Canada; ⁴Compound Properties, Xenon Pharmaceuticals Inc, Burnaby BC, Canada; ⁵Translational Drug Development, Xenon Pharmaceuticals Inc, Burnaby, Canada; ⁶Scientific Affairs, Xenon Pharmaceuticals, Inc, Burnaby BC, Canada; ⁷Executive Team, Xenon Pharmaceuticals Inc, Burnaby, Canada

*For correspondence: jpjohnson@xenon-pharma.com

Competing interest: [See page 21](#)

Funding: [See page 22](#)

Received: 24 July 2021
 Preprinted: [31 August 2021](#)
 Accepted: 23 February 2022
 Published: 02 March 2022

Reviewing Editor: Baron Chanda, Washington University in St. Louis, United States

© Copyright Johnson et al. This article is distributed under the terms of the [Creative Commons Attribution License](#), which permits unrestricted use and redistribution provided that the original author and source are credited.

Abstract NBI-921352 (formerly XEN901) is a novel sodium channel inhibitor designed to specifically target Na_v1.6 channels. Such a molecule provides a precision-medicine approach to target SCN8A-related epilepsy syndromes (SCN8A-RES), where gain-of-function (GoF) mutations lead to excess Na_v1.6 sodium current, or other indications where Na_v1.6 mediated hyper-excitability contributes to disease (Gardella and Møller, 2019; Johannesen et al., 2019; Veeramah et al., 2012). NBI-921352 is a potent inhibitor of Na_v1.6 (IC₅₀ 0.051 μM), with exquisite selectivity over other sodium channel isoforms (selectivity ratios of 756 X for Na_v1.1, 134 X for Na_v1.2, 276 X for Na_v1.7, and >583 X for Na_v1.3, Na_v1.4, and Na_v1.5). NBI-921352 is a state-dependent inhibitor, preferentially inhibiting inactivated channels. The state dependence leads to potent stabilization of inactivation, inhibiting Na_v1.6 currents, including resurgent and persistent Na_v1.6 currents, while sparing the closed/rested channels. The isoform-selective profile of NBI-921352 led to a robust inhibition of action-potential firing in glutamatergic excitatory pyramidal neurons, while sparing fast-spiking inhibitory interneurons, where Na_v1.1 predominates. Oral administration of NBI-921352 prevented electrically induced seizures in a *Scn8a* GoF mouse, as well as in wild-type mouse and rat seizure models. NBI-921352 was effective in preventing seizures at lower brain and plasma concentrations than commonly prescribed sodium channel inhibitor anti-seizure medicines (ASMs) carbamazepine, phenytoin, and lacosamide. NBI-921352 was well tolerated at higher multiples of the effective plasma and brain concentrations than those ASMs. NBI-921352 is entering phase II proof-of-concept

trials for the treatment of *SCN8A*-developmental epileptic encephalopathy (*SCN8A*-DEE) and adult focal-onset seizures.

Editor's evaluation

This exciting study reports on the characterization of a novel compound that preferentially targets Nav1.6 voltage-gated sodium channels and shows substantial activity against epilepsy associated *SCN8A* mutations and seizure activity in a variety of animal models. This compound and approach has significant promise to be translated into a therapeutic for individuals with treatment resistant epilepsy.

Introduction

Nav1.6 voltage-gated sodium channels are widely expressed in the brain and are important contributors to neural excitability (Meisler, 2019; Royeck et al., 2008). Mutations in the *SCN8A* gene result in malfunction of Nav1.6 sodium channels and cause a spectrum of *SCN8A*-related syndromes in humans, and disruptions of mouse Nav1.6 likewise disrupt normal physiology (Burgess et al., 1995; Gardella and Møller, 2019; Johannesen et al., 2019; Meisler, 2019; Veeramah et al., 2012; Wagnon et al., 2015). Variants of Nav1.6 channels can result in either gain or loss of function. Loss-of-function (LoF) variants in humans are generally associated with autism spectrum disorders with cognitive and developmental delay without epilepsy (Inglis et al., 2020; Liu et al., 2019), but, in some cases, can lead to late-onset seizures. In mice, LoF variants of Nav1.6 lead to motor impairment but increase seizure resistance (Hawkins et al., 2011; Martin et al., 2007). Gain-of-function (GoF) variants in human *SCN8A* generally result in early-onset *SCN8A*-related epilepsy syndromes (*SCN8A*-RES). The most severe of these epilepsy syndromes is *SCN8A* developmental and epileptic encephalopathy (*SCN8A*-DEE) (Gardella and Møller, 2019; Hammer et al., 2016; Johannesen et al., 2019). Most *SCN8A*-RES patients carry de novo heterozygous missense variants that lead to a gain of function of the Nav1.6 channel, although inherited and bi-allelic variants have been reported (Gardella and Møller, 2019; Wengert et al., 2019). *SCN8A*-DEE patients present early in life with seizure onset usually occurring in the first year of life. After seizure onset, patients begin to miss developmental milestones and display additional symptoms, including cognitive and motor delay, hypotonia, and cortical blindness. *SCN8A*-DEE individuals are predisposed to early death, including sudden unexplained death in epilepsy (SUDEP). While *SCN8A*-RES patients often have treatment-resistant seizures, many can achieve seizure reduction or seizure freedom upon treatment with anti-seizure medicines (ASMs) that non-selectively inhibit voltage-gated sodium channels, like phenytoin (Boerma et al., 2016; Braakman et al., 2017). *SCN8A*-RES patients may require doses that are higher than those prescribed for most epilepsy patients and, as a result, can be more prone to drug-related adverse events (Boerma et al., 2016; Gardella and Møller, 2019). Even with high doses and multiple ASMs, many patients continue to have uncontrolled seizures as well as extensive comorbidities. The aggressive pharmacotherapy required to protect *SCN8A* patients from life-threatening seizures often comes with attendant side effects that would not be tolerated in less severely impacted populations.

Existing sodium channel inhibitor ASMs are nonselective, blocking all voltage-gated sodium channel isoforms at similar plasma or brain concentrations. This lack of selectivity likely limits the benefits of sodium channel inhibitors since LoF variants of Nav1.1 are known to impair inhibitory interneuron function and cause generalized epilepsy with seizures plus (GEFS+) and *SCN1A*-DEE (Dravet Syndrome) (Catterall et al., 2010; Claes et al., 2001; Escayg et al., 2000; Gennaro et al., 2003). Thus, inhibiting Nav1.1 may counter the benefit of inhibiting the sodium channels of excitatory neurons. Inhibiting Nav1.4 and Nav1.5 currents is also undesirable since those channels are critical for facilitating contraction of skeletal and cardiac muscles, respectively (Chen et al., 1998; Ptáček et al., 1991; Rojas et al., 1991).

We hypothesized that a selective inhibitor of Nav1.6 could provide a safer and more effective treatment for patients with *SCN8A*-RES and might also be more broadly efficacious in more common forms of epilepsy. An extensive medicinal-chemistry effort produced NBI-921352, the first potent and selective inhibitor of Nav1.6 channels (Neurocrine, 2019). We explored the profile of NBI-921352 in vitro, ex vivo and in three preclinical in vivo rodent seizure models, including electrically induced seizure

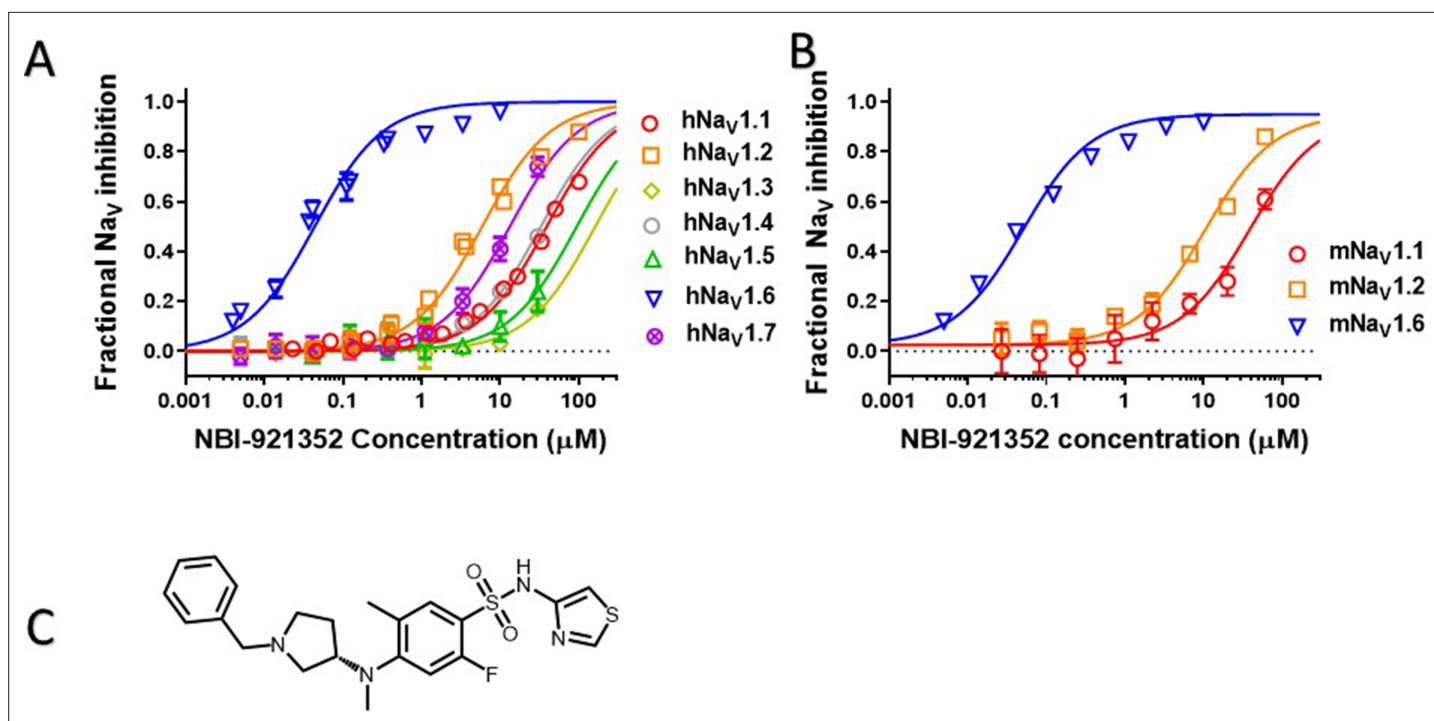


Figure 1. Potency and isoform selectivity of NBI-921352 for human and mouse Na_V channels. Concentration-response curves were generated by automated patch-clamp electrophysiology using the SophionQube. Concentration-response curves were generated for human (A) or mouse (B) Na_V channel isoforms heterologously expressed in HEK293 cells. The analysis included only those cells that met pre-specified acceptance criteria for seal quality, current amplitude, and series resistance. Normalized data from all cell recordings at a concentration were grouped together and plotted with GraphPad Prism 8. Details regarding the number of cells analyzed for each Na_V channel and concentration can be found in the source data sheet. Error bars indicating the standard error of the mean fraction were plotted for all points, but, in some cases, they were smaller than the data point symbols and, therefore, not visible. The chemical structure of NBI-921352 is shown (C).

The online version of this article includes the following source data and figure supplement(s) for figure 1:

Source data 1. Quantification of potency and isoform selectivity of NBI-921352.

Figure supplement 1. Representative raw traces of voltage-clamp recordings of control and the concentrations close to the NBI-921352 IC_{50} for all tested sodium channel isoforms in **Figure 1**.

Figure supplement 2. Potency of NBI-921352 measured from a holding potential approximating the $\text{V}_{0.5}$ of inactivation for Na_V1 .

Figure supplement 2—source data 1. Quantification of potency with alternate voltage protocol.

assays in genetically engineered mice bearing heterozygous *Scn8a* GoF $\text{Na}_V1.6$ channels (N1768D), as well as in wild-type mice and rats.

Results

In vitro Na_V potency and selectivity

Human Na_V channel isoforms $\text{hNa}_V1.1$, $\text{hNa}_V1.2$, $\text{hNa}_V1.3$, $\text{hNa}_V1.4$, $\text{hNa}_V1.5$, $\text{hNa}_V1.6$, and $\text{hNa}_V1.7$ were heterologously expressed in HEK-293 cells, and the potency and isoform selectivity of NBI-921352 (**Figure 1**, **Table 1**) was determined by automated patch-clamp techniques. NBI-921352 potently inhibited $\text{hNa}_V1.6$ channel currents with an inhibitory concentration 50% (IC_{50}) of 0.051 μM (95% CI: 0.030–0.073 μM ; $N = 3$) calculated from three biological replicates. Inhibition of other human $\text{Na}_V1.X$ isoforms required higher concentrations of NBI-921352 with IC_{50} 's of 39 μM (95% CI: 31–47 μM ; $N = 3$) for $\text{hNa}_V1.1$, 6.9 μM (95% CI: 1.6–12 μM ; $N = 3$) for $\text{hNa}_V1.2$, > 30 μM for $\text{hNa}_V1.3$, > 30 μM for $\text{hNa}_V1.4$, > 30 μM for $\text{hNa}_V1.5$, and 14 μM (95% CI: 6.4–22 μM ; $N = 3$) for $\text{hNa}_V1.7$. These potencies provide selectivity ratios for $\text{hNa}_V1.6$ versus the other hNa_V isoforms ($\text{IC}_{50} \text{ hNa}_V1.X / \text{IC}_{50} \text{ hNa}_V1.6$) of 756 ($\text{Na}_V1.1$), 134 ($\text{Na}_V1.2$), 276 ($\text{Na}_V1.7$) and >583 ($\text{Na}_V1.3$, $\text{Na}_V1.4$, $\text{Na}_V1.5$). Inhibition of $\text{Na}_V1.8$ and $\text{Na}_V1.9$ was not assessed since both channels are believed to be limited to peripheral sensory neurons and are not expected to have much impact on the efficacy and tolerability of sodium channel inhibitors

Table 1. Potency and isoform selectivity of NBI-921352 for human and mouse Na_v channels. Note that IC_{50} s for the neuronal sodium channels, Na_v 1.1, Na_v 1.2, and Na_v 1.6, have been more accurately defined than those for non-neuronal sodium channels. Explicit IC_{50} s for Na_v 1.3, Na_v 1.4, and Na_v 1.5 were not determined since the inhibition at the highest concentration tested (30 μM) was <50%. IC_{50} s are the mean of 3 separate biological replicates of the IC_{50} determinations for each channel. The error is shown as the 95% confidence interval of the mean IC_{50} . None of the other tested isoforms displayed IC_{50} s within the 95% confidence interval of the Na_v 1.6 IC_{50} and the confidence intervals were well separated as well.

	Na_v 1.6	Na_v 1.1	Na_v 1.2	Na_v 1.3	Na_v 1.4	Na_v 1.5	Na_v 1.7
Human IC_{50} (μM)	0.051	39	6.9	> 30	> 30	> 30	14
95% CI	0.030–0.073	31–47	1.6–12	-	-	-	6.4–22
Human Selectivity hNa_v 1.X / hNa_v 1.6	1	756	134	> 583	> 583	> 583	276
Mouse IC_{50} (μM)	0.058	41	11				
Mouse Selectivity mNa_v 1.X / mNa_v 1.6	1	709	191				

in epilepsy. Inhibition of Na_v 1.8 and Na_v 1.9 might reduce pain perception, but this would not be considered a significant liability for an anti-seizure medicine.

Since we intended to evaluate *in vivo* effects of NBI-921352 in mouse seizure models, we also assessed the potency of NBI-921352 in the mouse Na_v isoforms that are most highly expressed in the brain, Na_v 1.6, Na_v 1.1, and Na_v 1.2. The potency and selectivity in mouse Na_v channels closely paralleled that seen in the human orthologues with IC_{50} s of 0.058 μM (95% CI: 0.046–0.070 μM ; N = 3) for mNa_v 1.6, 41 μM (95% CI: 30–52 μM ; N = 3) for mNa_v 1.1, and 11 μM (95% CI: 8.2–14 μM ; N = 3) for mNa_v 1.2. Selectivity ratios (IC_{50} mNa_v 1.X / IC_{50} mNa_v 1.6) were 709 (Na_v 1.1), and 191 (Na_v 1.2). These data indicate that NBI-921352 potently inhibits both human and mouse Na_v 1.6 channels, and that it does so at concentrations \geq 134 fold lower than for any of the other channel isoforms tested.

NBI-921352 inhibited patient-identified variants of Na_v 1.6 channels

Patients with *SCN8A*-RES carry missense variants in the Na_v 1.6 channel. A great number of variants have been identified, with a range of biophysical defects. Since most variants are *de novo*, many have been identified in only one or a few patients. For this reason, we determined the effectiveness of NBI-921352 to inhibit nine patient identified variants spread across the channel (**Figure 2, Table 2; Gardella and Møller, 2019; Wagon and Meisler, 2015**). The nine variants studied have all been identified in *SCN8A*-RES patients and are in Domains II, III, IV, and the C-terminus. Inhibition of the mutant channel constructs was evaluated by automated patch-clamp electrophysiological techniques after transient transfection of the human Na_v 1.6 variant construct of interest into Expi293F cells. All the variants were sensitive to inhibition by NBI-921352. Observed IC_{50} s for inhibition were 0.051 μM (WT mean from **Figure 1**), 0.031 μM (95% CI: 0.027–0.037 μM)(T767I), 0.021 μM (95% CI: 0.017–0.026 μM)(R850Q), 0.032 μM (95% CI: 0.029–0.036 μM)(N984K), 0.035 μM (95% CI: 0.029–0.043 μM)(I1327V), 0.039 μM (95% CI: 0.031–0.050 μM)(N1466K), 0.34 μM (95% CI: 0.26–0.44 μM)(R1617Q), 0.055 μM (95% CI: 0.046–0.064 μM)(N1768D), 0.068 μM (95% CI: 0.054–0.085 μM)(R1872W), and 0.035 μM (95% CI: 0.029–0.041 μM)(N1877S). We found that eight of the nine variants were inhibited with a potency similar to that of the wild-type channel, with most being slightly more potently inhibited. Only one variant, R1617Q, required markedly higher concentrations of NBI-921352 for inhibition, with an IC_{50} for inhibition 6.6-fold higher than that of the wild-type Na_v 1.6 channel. The reduced potency for R1617Q is consistent with the variant residing in the predicted binding site of NBI-921352 in the domain IV voltage sensor, see discussion.

NBI-921352 is a state-dependent inhibitor

Many small molecule inhibitors of Na_v channels bind preferentially to open and or inactivated states (**Bean et al., 1983; Courtney et al., 1978; Strichartz, 1976**).

Na_v inhibitors that are structurally similar to NBI-921352 are known to act by binding to the VSD4 in the 'UP' position and hence stabilize inactivated states (**Ahuja et al., 2015; McCormack et al., 2013**). Charge movement in VSD4 has been linked to the voltage dependence of fast inactivation (**Ahern**

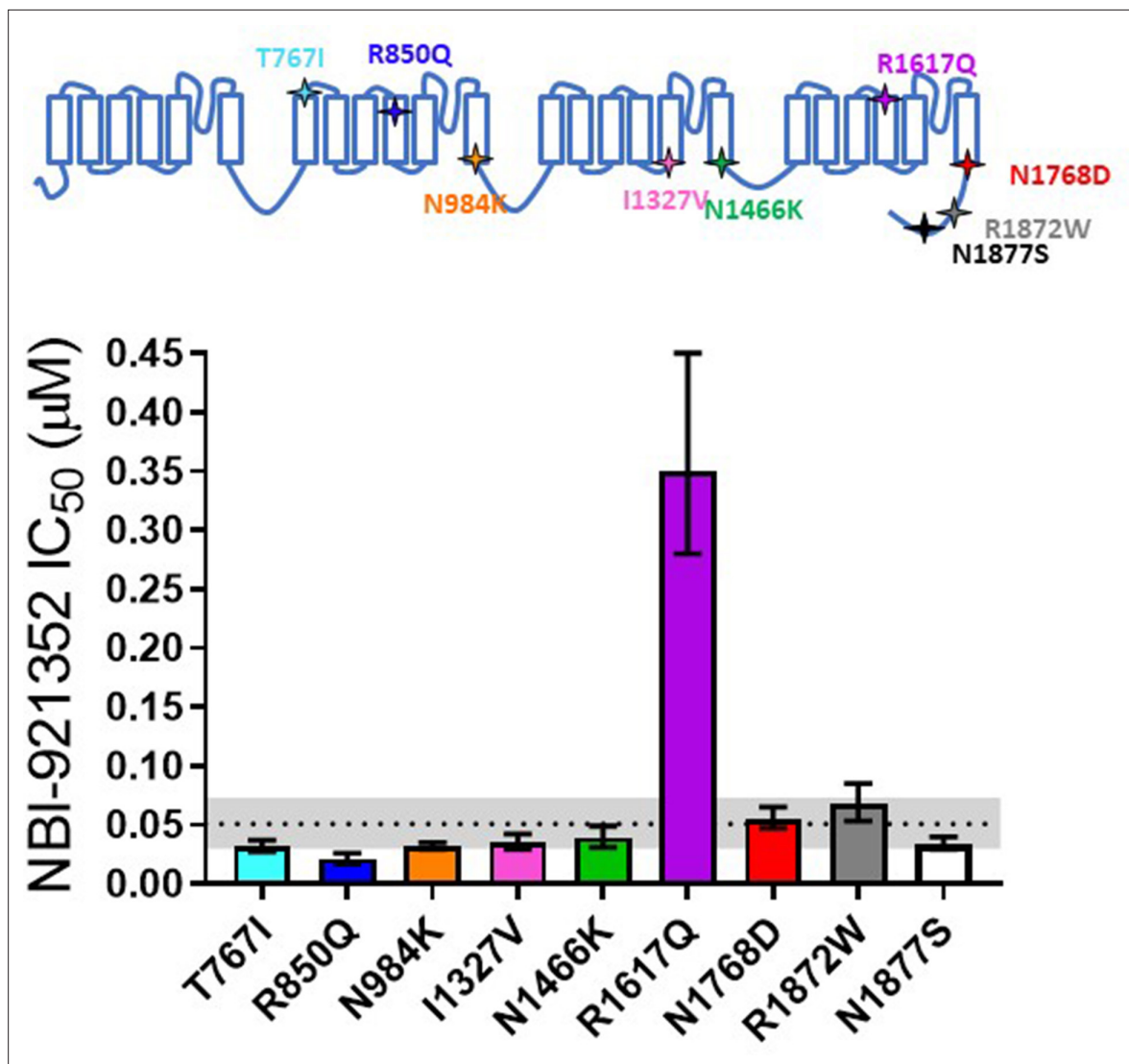


Figure 2. Comparison of NBI-921352 potency on human wild-type $\text{Na}_v1.6$ and patient-identified variants of $\text{Na}_v1.6$. All constructs were transiently transfected into Expi293F cells and evaluated by automated patch-clamp electrophysiology using the SophionQube. The voltage-clamp methods were identical to those used for evaluation of the wild-type channels. The error bars indicate the 95% confidence interval of the fitted IC_{50} generated in Prism. The horizontal dotted line is at the IC_{50} for wild type $\text{Na}_v1.6$ (51 nM, see **Figure 1**). The gray shaded band indicates the 95% confidence range for the IC_{50} for wild-type $\text{Na}_v1.6$. Only two variants have fitted IC_{50} 's outside of the 95% confidence interval for the wild-type channel IC_{50} . R850Q was slightly more potently inhibited and R1617Q was less potently inhibited than the wild-type channel. R1617Q is near the proposed binding site for NBI-921352.

The online version of this article includes the following source data for figure 2:

Source data 1. Quantification inhibition of patient variants.

et al., 2016). It is likely that the anionic aryl sulfonamide headgroup of NBI-921352 interacts with the fourth arginine in S4 of VSD4 and prevents return of VSD4 to the rested position and recovery from inactivation as seen for related compounds (*Ahuja et al., 2015*). For these reasons, we expect that binding will be encouraged by VSD4 residing in the UP, inactivated, state.

We designed our voltage-clamp protocols to encourage high occupancy of inactivated states by holding at depolarized membrane potentials (−45 mV for $\text{Na}_v1.1$, $\text{Na}_v1.2$, $\text{Na}_v1.3$, $\text{Na}_v1.4$, and $\text{Na}_v1.6$). The isoforms that inactivate at the most negative membrane potentials ($\text{Na}_v1.5$ and $\text{Na}_v1.7$) accumulate excess slow inactivation at −45 mV, reducing the signal size. For these two isoforms, the membrane potential was held at −60 mV to preserve robust assay performance while fully inactivating the channels. Our investigation into the state dependence of NBI-921352 did not attempt to

Table 2. Comparison of NBI-921352 potency on human wild-type $\text{Na}_v1.6$ and patient-identified gain-of-function variants of $\text{Na}_v1.6$. IC_{50} s corresponding to **Figure 2** are shown in the table and were calculated as indicated for **Table 1**. The 95% confidence intervals are those determined by the fit of the IC_{50} in Prism.

	WT	T767I	R850Q	N984K	I1327V	N1466K	R1617Q	N1768D	R1872W	N1877S
h $\text{Na}_v1.6$ IC_{50} (μM)	0.051	0.031	0.021	0.032	0.035	0.039	0.349	0.054	0.067	0.034
95% CI	0.030–0.073	0.027–0.037	0.017–0.026	0.029–0.035	0.029–0.042	0.031–0.049	0.28 to 0.40	0.047–0.065	0.053–0.085	0.029–0.040
Fold change WT / Variant	-	0.6	0.4	0.6	0.7	0.8	6.8	1.1	1.3	0.7

rigorously differentiate binding to open channels versus fast inactivated or fast inactivated versus slow inactivated states.

To query the state dependence of NBI-921352, we measured the apparent potency with two different voltage protocols that favor either the closed (rested) state or inactivated states (**Figure 3**). Holding the membrane potential at -120 mV induces most channels to reside in the resting state. Brief depolarizations to measure $\text{Na}_v1.6$ current enabled the determination of an IC_{50} of $36 \mu\text{M}$ (95% CI: 29 – $47 \mu\text{M}$) for rested-state channels. Holding the membrane potential at -45 mV encourages channels

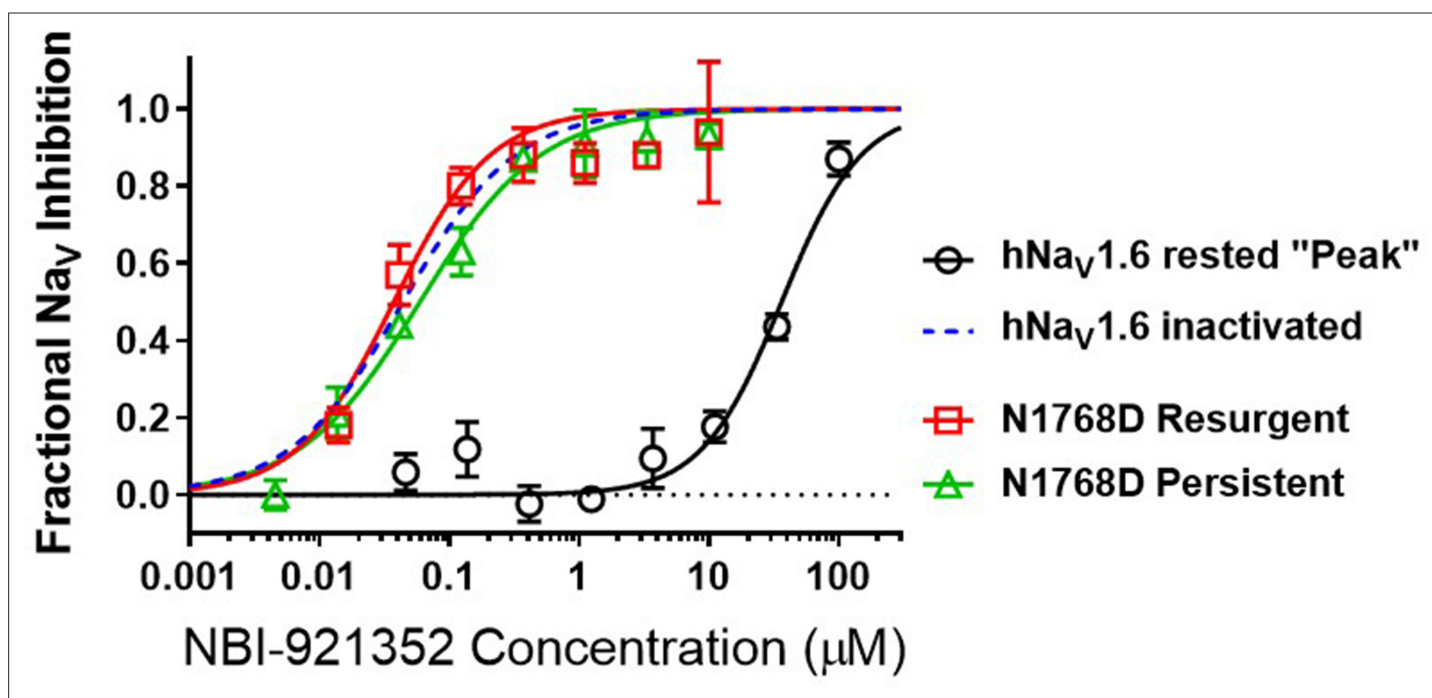


Figure 3. NBI-921352 is a state-dependent inhibitor of $\text{Na}_v1.6$ and preferentially targets inactivated channels. Concentration-response curves were generated for human WT and N1788D channel isoforms heterologously expressed in HEK293 cells. The analysis included only those cells that met pre-specified acceptance criteria for seal quality, current amplitude, and series resistance. Normalized data from all cell recordings at a concentration were pre-grouped together and plotted with GraphPad Prism 8. Details regarding the number of cells analyzed for each Na_v channel isoform and concentration can be found in the source data sheet. Error bars indicating the standard error of the mean fraction were plotted for all points. The blue dotted line indicates the concentration-response curve for wild-type $\text{Na}_v1.6$ from **Figure 1**. When $\text{Na}_v1.6$ channels were equilibrated with NBI-921352 at voltages that allow equilibration with inactivated states (-45 mV), the compound provided potent inhibition, as seen in **Figure 1**. NBI-921352 also exhibited potent block of $\text{Na}_v1.6$ when measuring persistent or resurgent sodium current using distinct voltage protocols (see Materials and methods and text). Forcing channels to the rested, closed state by hyperpolarizing to -120 mV resulted in very weak inhibition. Current evoked from very negative potentials is sometimes referred to as 'peak current'. The 95% confidence intervals for the IC_{50} s reported in the results are those provided for the error of the fit by Prism.

The online version of this article includes the following source data and figure supplement(s) for figure 3:

Source data 1. Quantification of state dependence of NBI-921352.

Figure supplement 1. Representative raw traces of the $\text{Na}_v1.6$ currents used to generate the summary data in **Figure 3**.

to transition into inactivated states. Brief hyperpolarizations allow rapid recovery from inactivation for channels that are not bound to drug followed by a short 20ms test pulse to -20 mV to measure currents from unbound channels (see Materials and methods for details). Measuring the ability of NBI-921352 to inhibit reopening of activated channels leads to an apparent IC_{50} of 0.051 μ M (**Figures 1 and 3**). Thus, NBI-921352 strongly prefers inactivated channels, inhibiting them at concentrations more than 750-fold less than those needed to inhibit rested or 'peak' sodium currents.

At more hyperpolarized potentials, potency for all isoforms will tend to be somewhat less. Nonetheless potency on $Na_v1.6$ at a more physiologic potential (-62 mV) is shown in **Figure 1—figure supplement 2** where the push towards inactivated states is not so strong. NBI-921352 remains potent ($IC_{50}0.053$ μ M) in this assay, suggesting that potency and selectivity under physiologic conditions will remain high.

NBI-921352 inhibited persistent and resurgent currents from mutant $Na_v1.6$ channels

The state-dependent nature of inhibition is also revealed in other types of voltage-clamp protocols, including those designed to measure persistent or resurgent sodium currents. Some drugs or candidate drugs, like PRAX-330 and Riluzole, have been touted based on their preference for persistent currents, but this appears to be a feature of many of the compounds in the Na_v inhibitor class since they are generally poor inhibitors of closed/rested state channels and bind preferentially to activated channels (**Colombo et al., 2013; Mason et al., 2019; Wengert and Patel, 2021**). Apparent differences in persistent current selectivity are largely driven by differential kinetics and concentration dependences in combination with the electrophysiological protocols chosen for the measurements.

Elevated persistent and or resurgent currents are believed to underlie or contribute to the pathology of many sodium channel related pathologies (**Mason et al., 2019; Pan and Cummins, 2020; Potet et al., 2020; Tidball et al., 2020; Zaman et al., 2019**). In most conditions, normal $Na_v1.6$ channels inactivate rapidly and nearly completely after opening. Persistent currents result from channels that are not stably inactivated – a common phenotype for epilepsy-inducing variants in $Na_v1.6$, including N1768D (**Tidball et al., 2020; Wagnon et al., 2015**). We found that NBI-921352 inhibited N1768D $Na_v1.6$ persistent currents (measured as the non-inactivating current 10ms after initiation of the depolarizing test pulse) with a similar potency as for activated wild-type $Na_v1.6$ channels with an IC_{50} of 0.059 μ M (95% CI: 0.044 – 0.082 μ M) (**Figure 3**). A more traditional approach to measuring persistent currents is to step from a very hyperpolarized voltage (for example -120 mV) to a strong depolarization for 50ms or longer. This approach is not viable for NBI-921352 since equilibration of block after from such negative, non-physiological, voltages takes several seconds.

Resurgent currents occur after repolarizing following a strong depolarization as channels redistribute between closed, open, and inactivated states (**Raman and Bean, 1997**). These resurgent currents are enhanced in many SCN8A-RES variants (**Pan and Cummins, 2020; Raman et al., 1997**). NBI-921352 also effectively inhibited resurgent currents from N1768D channels with apparent IC_{50} of 0.037 μ M (95% CI: 0.025 – 0.060 μ M). While the resurgent currents cannot be measured with the same voltage protocols used to measure inactivated state inhibition, these data indicate that N1768D $Na_v1.6$ resurgent currents are susceptible to inhibition by NBI-921352 and that inhibition occurs at similar concentrations.

NBI-921352 preferentially inhibited excitatory pyramidal neurons and spared inhibitory interneurons

A primary goal of creating $Na_v1.6$ selective inhibitors was to spare $Na_v1.1$, the voltage-gated sodium channel that is most prevalent in inhibitory interneurons. This should allow the selective targeting of excitatory neurons, where $Na_v1.6$ and $Na_v1.2$ are believed to be dominant, over inhibitory interneurons. To test this hypothesis, we performed current-clamp experiments in glutamatergic pyramidal neurons from mouse layer five neocortex and from fast spiking interneurons in the same region. Application of 0.250 μ M NBI-921352 decreased the maximum firing rate in all three pyramidal neurons tested (**Figure 4A**). The difference in the cumulative area under the curves (AUC) for control versus NBI-921352 treated conditions was evaluated by a paired two tailed t-test ($N = 3$ or 4 cells for each point). Current injection levels > 160 pA led to a significant reduction of the cumulative area under the input output curve ($p < 0.05$ in a paired two-tailed t-tests) relative to the control condition. Specific

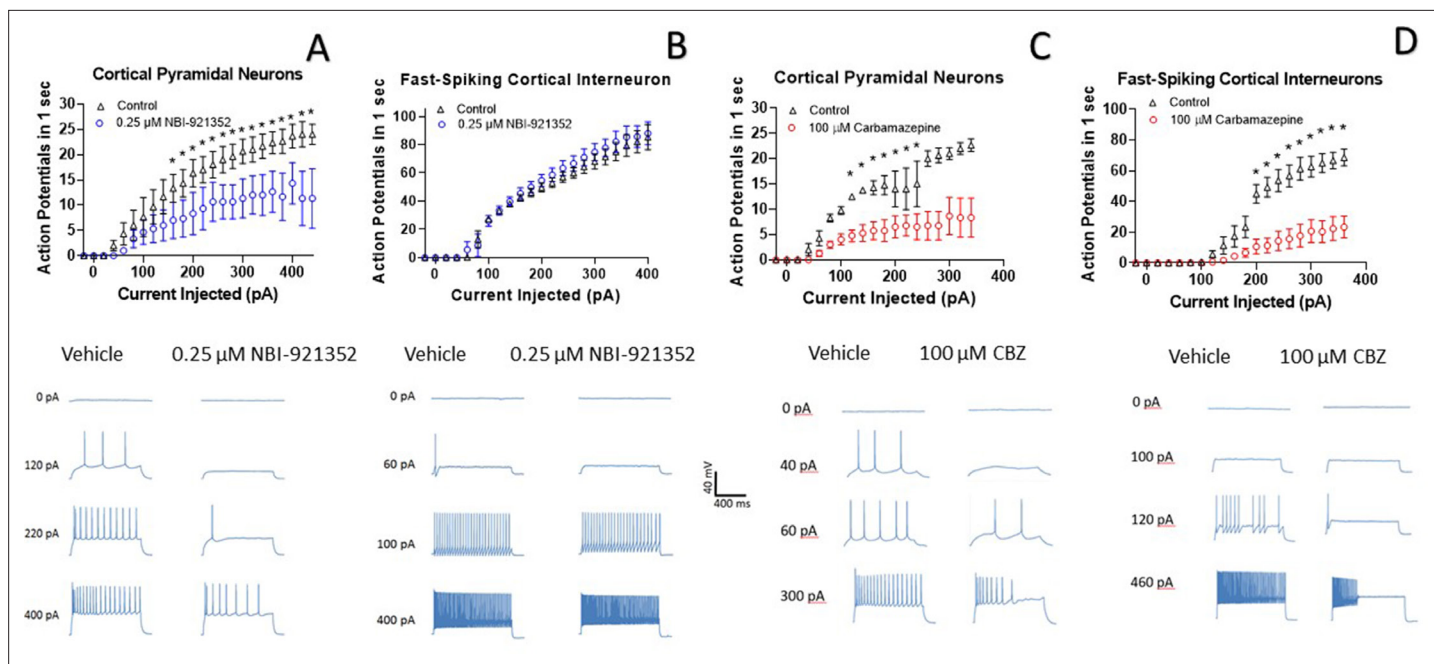


Figure 4. NBI-921352 inhibits firing in pyramidal neurons but spares fast-spiking interneurons. Current input versus action-potential output evaluations in wild-type mouse brain slices treated with vehicle or 0.25 μM NBI-921352 (A & B), or 100 μM carbamazepine (C & D) was plotted. In cortical pyramidal neurons, both NBI-921352 (A) and carbamazepine (C) reduced action-potential spiking. In fast-spiking cortical interneurons, treatment with NBI-921352 resulted in a trend toward slightly increased firing frequency (B), while carbamazepine markedly reduced firing (D). The main upper panels compare average action-potential count of 3–4 neurons in each condition \pm the standard error of the mean. The lower panels show recordings for individual representative neurons for each condition. No inhibitors of synaptic inputs were used for these experiments. The difference in the cumulative area under the curves (AUC) for control versus NBI-921352 treated conditions was evaluated by a paired two tailed t-test ($N = 3$ or 4 cells for each point). *Indicates a $p < 0.05$ relative to the control condition. Specific p values are shown in the data transparency Excel file. See **Figure 4—figure supplement 1** for more individual neuron comparisons.

The online version of this article includes the following source data and figure supplement(s) for figure 4:

Source data 1. Quantification of cortical neuron current clamp input output.

Figure supplement 1. Results for each tested neuron for the neurons summarized in **Figure 4**.

Figure supplement 1—source data 1. Quantification of individual neurons.

p values are shown in the data transparency Excel file. See **Figure 4—figure supplement 1** for more individual neuron comparisons.

In contrast, NBI-921352 had no significant effect on the fast-firing inhibitory interneurons tested (**Figure 4B**). Carbamazepine significantly inhibited action-potential firing in both pyramidal neurons and in fast-spiking interneurons and the degree of inhibition was similar in both types of neurons. A before and after comparison for all tested neurons is shown in **Figure 4—figure supplement 1**.

NBI-921352 inhibited electrically induced seizures in *Scn8a*^{N1768D/+} mice

A selective inhibitor of $\text{Na}_v1.6$ should lend itself to the treatment of disease states caused by pathologic gain of function of $\text{Na}_v1.6$ channels. Hence, we examined the ability of NBI-921352 to inhibit electrically induced seizures in mice with a patient-identified GoF variant in the *Scn8a* gene encoding $\text{Na}_v1.6$. N1768D is a variant of $\text{Na}_v1.6$ identified in the first reported *SCN8A*-DEE patient (**Veeramah et al., 2012**). N1768D $\text{Na}_v1.6$ channels have impaired voltage-dependent inactivation gating that results in persistent sodium currents and enhanced resurgent currents. Because $\text{Na}_v1.6$ channels are highly expressed in the neurons of the brain, increased sodium flux in excitatory neurons leads to seizures. Genetically modified mice bearing the same variant (*Scn8a*^{N1768D/+}) were created and found to be seizure prone, producing a mouse model with a similar phenotype as that observed in *SCN8A*-DEE patients (**Wagon et al., 2015**). Some *Scn8a*^{N1768D/+} mice develop spontaneous seizures at age p60

to p100, but seizure onset and frequency is quite variable, making spontaneous seizure studies challenging. In addition, mice rapidly clear NBI-921352, making it extremely difficult to maintain drug plasma and brain levels in an efficacious range for chronic or subchronic dosing experiments. NBI-921352 is more stable in humans with a half-life of elimination of approximately 8.5 hr (Beatch et al., 2020).

As an alternative means of assessing NBI-921352's ability to engage $\text{Na}_v1.6$ channels in vivo, we designed a modified version of the 6 Hz psychomotor seizure assay in *Scn8a*^{N1768D/+} mice (Barton et al., 2001; Focken et al., 2019). A mild current stimulation (12 mA) evoked robust generalized tonic-clonic seizures (GTC) with hindlimb extension in *Scn8a*^{N1768D/+} mice, but not in wild-type littermates.

Oral administration of NBI-921352 2 hr prior to electrical stimulation prevented induction of GTC with hindlimb extension in *Scn8a*^{N1768D/+} mice in a dose-dependent manner with a 50% effective dose (ED₅₀) of 15 mg/kg (95% CI 9.6–23 mg/kg, see Figure 5A).

After seizure assessment, all animals were euthanized, and the concentration of NBI-921352 was determined in the plasma and brain tissue from each mouse. The average concentrations for each dose group were used to generate plasma concentration and brain concentration versus efficacy relationships (Figure 5B and C, respectively). The plasma 50% effective concentration (EC₅₀) was 0.037 μM (95% CI 0.018–0.090 μM , see Figure 5B). The brain EC₅₀ was 0.064 μM (95% CI 0.045–0.091 μM , see Figure 5C).

NBI-921352 inhibited electrically induced seizures in wild-type mice

$\text{Na}_v1.6$ is an important mediator of neuronal excitability even in animals without GoF mutations. For this reason, we wondered whether NBI-921352 might have broader application in epilepsy beyond SCN8A-RES and in other syndromes of neural hyperexcitability. To gain insight into this possibility, we assessed NBI-921352 in a MES assay induced by direct-current electrical stimulus (DC-MES, see Materials and methods) in wild-type mice. Figure 5D and E & F show that NBI-921352 prevented GTC with hindlimb extension induction in the DC-MES assay in a dose- and concentration-dependent manner. The ED₅₀ for NBI-921352 was 23 mg/kg (95% CI 16–34 mg/kg, see Figure 5D). The efficacy of NBI-921352 was also concentration dependent with a plasma EC₅₀ of 0.52 μM (95% CI 0.25–1.2 μM , see Figure 5E) and a brain EC₅₀ of 0.20 μM (95% CI 0.12–0.38 μM , see Figure 5F).

NBI-921352 inhibited electrically induced seizures in wild-type rats

To further explore the preclinical efficacy of NBI-921352, we assessed NBI-921352 in a MES assay induced by direct-current electrical stimulus in wild-type Sprague Dawley rats (see Materials and methods). Figure 5G & H show that NBI-921352 prevented GTC with hindlimb-extension induction in the rat DC-MES assay in a dose- and concentration-dependent manner. The ED₅₀ for NBI-921352 was 3.7 mg/kg (95% CI 2.3–7.6 mg/kg, see Figure 5G). The efficacy of NBI-921352 was also concentration dependent with a plasma EC₅₀ of 0.15 μM (95% CI 0.09–0.31 μM , see Figure 5H) and a brain EC₅₀ of 0.037 μM (95% CI 0.028–0.054 μM , see Figure 5I).

Repeated-dosing efficacy in mice and rats

We found that repeated dosing tended to increase efficacy at lower doses and exposures of NBI-921352 than after a single dose (Figure 5, red symbols). Animals were dosed every 12 hr, morning, and evening for 13 doses. Two hours after the 13th dose, on the seventh day, efficacy was tested as in acute-dosing studies. A trend toward improved efficacy was noted in all three assays (see red symbols in Figure 5), but the improvement was not statistically significant when comparing single-dose groups to repeated-dose groups at the same dose level in the same experiment. NBI-921352 did not appreciably accumulate in the plasma or tissue and therefore any trends in improved efficacy were not explained by higher drug concentrations.

NBI-921352 is effective at lower brain concentrations than three Na_v inhibitor ASMs

The efficacy of Na_v inhibitors in epilepsy is presumed to be due to the drugs' action in the CNS, and CNS side effects are also commonly reported for this class of drugs (Walia et al., 2004). Hence brain concentrations are likely to drive both efficacy and many adverse events. We found that NBI-921352 was effective in the three preclinical seizure models evaluated at markedly lower brain concentrations

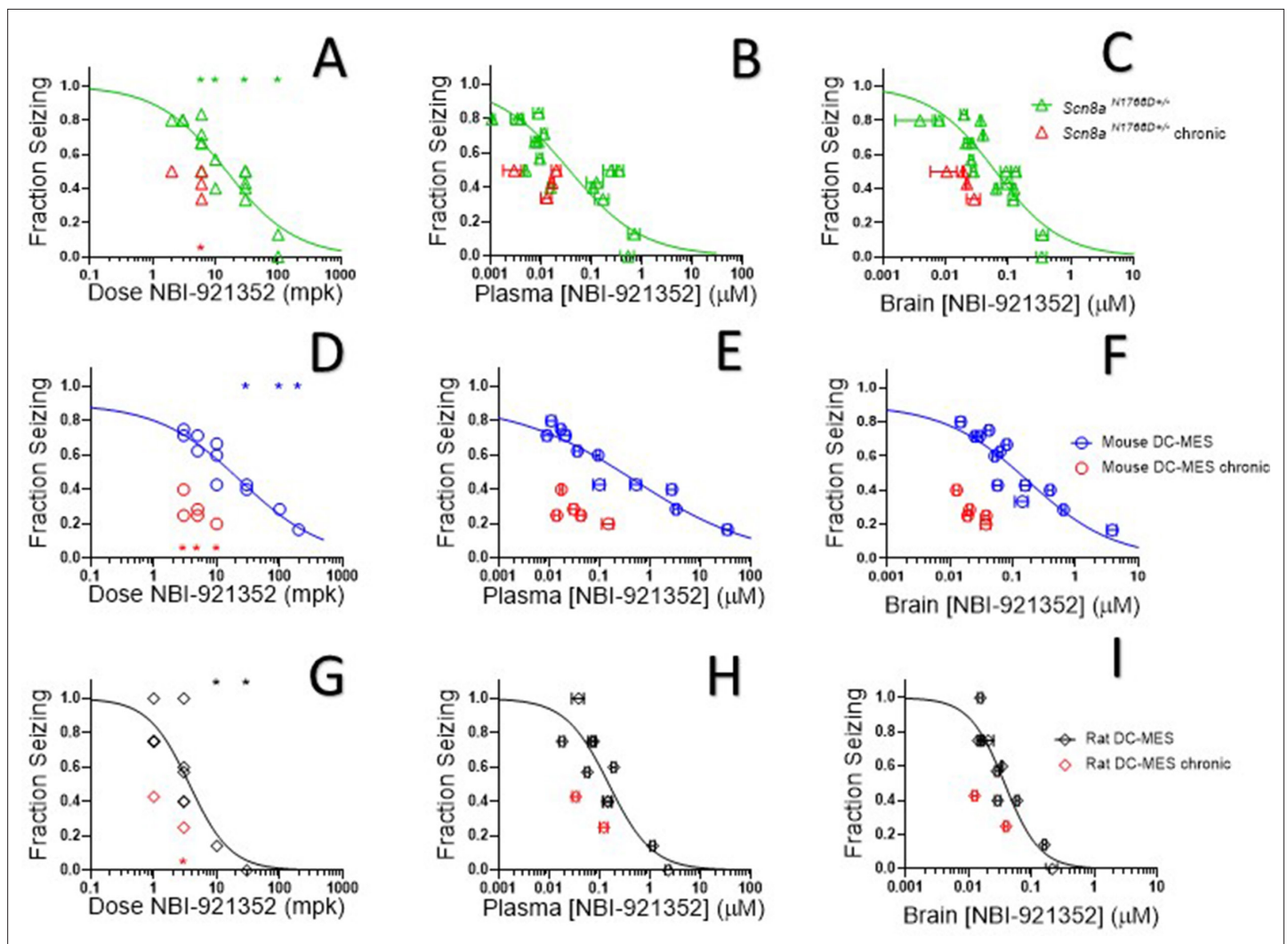


Figure 5. NBI-921352 inhibited electrically induced seizures in rodents. Dose of NBI-921352 is plotted versus efficacy in *Scn8a*^{N1768D/+} mice in the modified 6 Hz psychomotor seizure assay in A. Plasma concentration of NBI-921352 is plotted versus efficacy in *Scn8a*^{N1768D/+} mice in the modified 6 Hz psychomotor seizure assay in B. Brain concentration of NBI-921352 is plotted versus efficacy in *Scn8a*^{N1768D/+} mice in the modified 6 Hz psychomotor seizure assay in C. Green open triangles represent data from animals that received a single dose 2 hr before testing in the seizure assay. Red open triangles represent data from animals that received two daily doses (once every 12 hr) for 6 days. On day 7, these animals were given a final dose (the 13th dosing) 2 hr before testing in the seizure assay. Dose of NBI-921352 is plotted versus efficacy in wild-type mice in the DC-MES assay in D. Plasma concentration of NBI-921352 is plotted versus efficacy in wild-type mice in the DC-MES assay in E. Brain concentration of NBI-921352 is plotted versus efficacy in wild-type mice in the DC-MES assay in F. Blue open circles represent data from animals that received a single dose 2 hr before testing in the seizure assay. Red open circles represent data from animals that received two daily doses (once every 12 hr) for 6 days. On day seven these animals were given a final dose (the 13th dosing) 2 hr before testing in the seizure assay. Dose of NBI-921352 is plotted versus efficacy in wild-type rats in the DC-MES assay in G. Plasma concentration of NBI-921352 is plotted versus efficacy in wild-type rats in the DC-MES assay in H. Brain concentration of NBI-921352 is plotted versus efficacy in wild-type rats in the DC-MES assay in I. Black open diamonds represent data from animals that received a single dose 2 hr before testing in the seizure assay. Red open diamonds represent data from animals that received two daily doses (once every 12 hr) for 6 days. On day 7, these animals were given a final dose (the 13th dose) 2 hr before testing in the seizure assay. Each point represents the fraction of animals exhibiting a GTC with hindlimb extension after stimulus from a dosing group of six to eight animals. Horizontal error bars show the standard error of the mean plasma (B, E, H) or brain (C, F, I) concentrations measured from the animals in that dosing group immediately after assay. Where error bars are not visible, they are smaller than the symbols. No error bars are shown for the dose levels (A, D, G), since those were dictated by the experimenter. Groups receiving the same dose level were combined for statistical analysis. Between-group differences were compared to vehicle response and were analyzed using a Kruskal-Wallis test followed by Dunn's multiple comparisons test. Statistical significance was reached at values of $p < 0.05$ and is indicated by the stars at the top of A, D, and G. For specific p values and more details see **Figure 5—figure supplement 1**. Symbols in red represent animals tested after twice daily dosing for 6.5 days (see description above). Statistical analysis was completed as above for comparison between NBI-921352 treated and vehicle treated groups, and significance is indicated by a red star above the x-axis. In some cases, dose levels that were not statistically significant after a single dose became significant after repeat dosing when compared to vehicle controls. However, in no case were the groups treated with repeatedly

Figure 5 continued on next page

Figure 5 continued

with NBI-921352 statistically significant relative to their single dose comparison groups from the same experiment. For more data and p-values see **Figure 5—figure supplement 2**.

The online version of this article includes the following source data and figure supplement(s) for figure 5:

Source data 1. Quantification of impact of NBI-921352 on rodent seizures.

Figure supplement 1. Dose response and statistical analysis of the NBI-921352 dose groups for which brain and plasma concentration response curves are shown in **Figure 5**.

Figure supplement 2. Comparison of single dose versus sub-chronic dosing for NBI-921352.

than carbamazepine, phenytoin, and lacosamide (**Figure 6**). The brain EC_{50} s for carbamazepine were 9.4 μ M, 44 μ M, and 36 μ M for the *Scn8a*^{N1768D/+} 6 Hz model, WT mouse DC-MES, and WT rat DC-MES models, respectively. The brain EC_{50} s for phenytoin were 18 μ M, 13 μ M, and 2.6 μ M for the *Scn8a*^{N1768D/+} 6 Hz model, WT mouse DC-MES, and WT rat DC-MES models, respectively. The brain EC_{50} s for lacosamide were 3.3 μ M, 7.1 μ M, and 4.3 μ M for the *Scn8a*^{N1768D/+} 6 Hz model, WT mouse DC-MES, and WT rat DC-MES models, respectively. The lower brain concentrations required for efficacy with NBI-921352 are consistent with the potent inhibition of Na_v1.6 produced by NBI-921352 (**Figure 1**).

NBI-921352 provided improved separation between efficacy in rats and behavioral signs

The intent of creating a highly selective Na_v1.6 antagonist was to reproduce or improve on the efficacy of classic, nonselective, sodium channel inhibitor drugs while reducing or preventing the adverse events caused by polypharmacy with other sodium channel and non-sodium channel targets. If sparing Na_v1.1 and other off-target interactions does, in fact, reduce adverse events, then even higher receptor occupancy of Na_v1.6 might be achievable, thereby further improving efficacy.

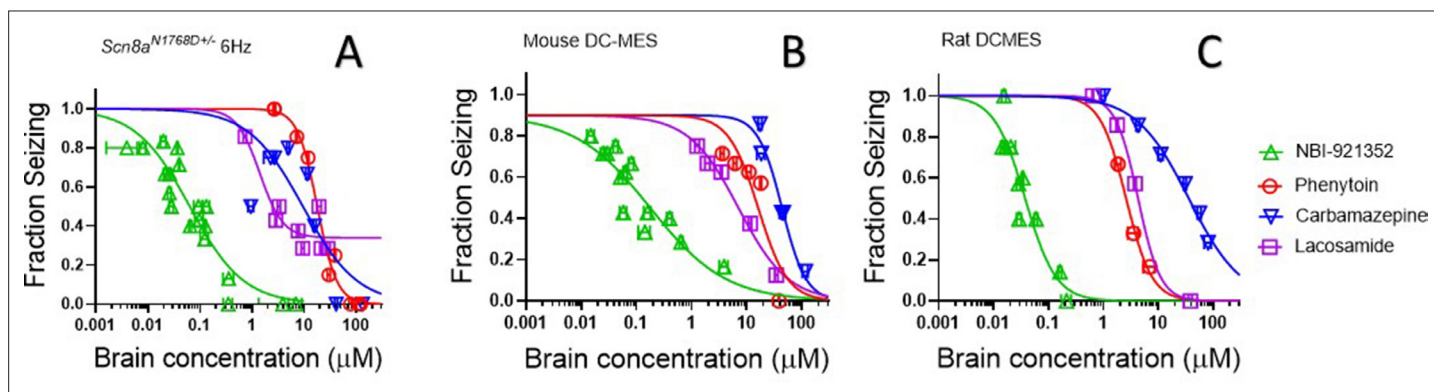


Figure 6. NBI-921352 is more potent than three commonly prescribed Na_v inhibitor ASMs. Brain concentration versus fraction of animals exhibiting is plotted for NBI-921352 versus that for phenytoin, carbamazepine, and lacosamide in the *Scn8a*^{N1768D/+} modified 6 Hz model (**A**), the wild-type mouse DC-MES model (**B**), and the wild-type rat DC-MES model (**C**). Each point represents the fraction of animals exhibiting a GTC with hindlimb extension after stimulus from a dosing group of six to eight animals. Horizontal error bars show the standard error of the mean brain concentrations measured from the animals in that dosing group immediately after assay. Where error bars are not visible, they are smaller than the symbols. Statistical analysis of significance of the dose groups for the concentrations shown were performed as in **Figure 5** and can be found in **Figure 5—figure supplement 1** (NBI-921352), **Figure 6—figure supplement 1** (Carbamazepine), **Figure 6—figure supplement 2** (Phenytoin), and **Figure 6—figure supplement 3** (Lacosamide).

The online version of this article includes the following source data and figure supplement(s) for figure 6:

Source data 1. Quantification of effective brain concentrations of NBI-921352 versus common AEDs.

Figure supplement 1. Dose response and statistical analysis of the Carbamazepine dose groups for which brain and plasma concentration response curves are shown in **Figures 6 and 7** respectively.

Figure supplement 2. Dose response and statistical analysis of the Phenytoin dose groups for which brain and plasma concentration response curves are shown in **Figures 6 and 7** respectively.

Figure supplement 3. Dose response and statistical analysis of the Lacosamide dose groups for which brain and plasma concentration response curves are shown in **Figures 6 and 7** respectively.

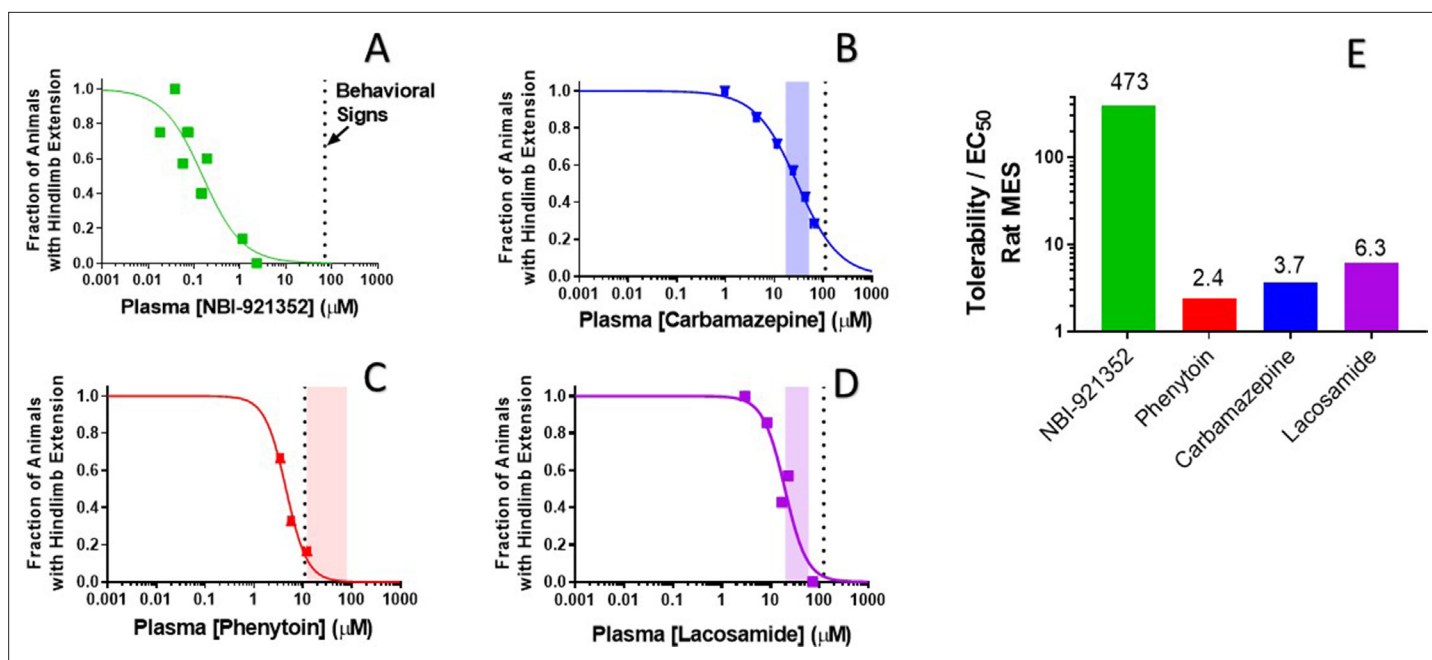


Figure 7. Rat efficacy compared to acute tolerability for NBI-921352 relative to Na_v inhibitor ASMs. Plasma concentration versus efficacy data is shown for the rat DC-MES assay for NBI-921352 (A), carbamazepine (B), phenytoin (C), and lacosamide (D). The vertical dotted lines indicate the lowest plasma concentration at which a rat was observed to exhibit atypical behavioral signs indicative of an adverse reaction to drug in the assay format. Animals exhibiting such signs were excluded from efficacy evaluation. The shaded bars in B, C, and D indicate the approximate human plasma concentrations observed in clinical practice. Panel E shows the ratio of the (rat plasma EC_{50} / the plasma concentration where behavioral signs were noted for each compound). Statistical analysis of significance of the dose groups for the concentrations shown can be found in **Figure 5—figure supplement 1** (NBI-921352), **Figure 6—figure supplement 1** (Carbamazepine), **Figure 6—figure supplement 2** (Phenytoin), and **Figure 6—figure supplement 3** (Lacosamide).

The online version of this article includes the following source data for figure 7:

Source data 1. Quantification of effective and tolerated plasma concentrations of NBI-921352 versus common AEDs.

To evaluate our hypothesis, we compared the window between the plasma concentrations required for efficacy (plasma EC_{50}) relative to the minimal plasma concentration at which treated rats showed behavioral signs of adverse effects as reported by the blinded experimenter (**Figure 7**). We made this comparison both for NBI-921352 and for several widely used Na_v inhibitor ASMs: carbamazepine, phenytoin, and lacosamide.

NBI-921352 was well tolerated in these studies up to a plasma concentration of 71 μM . Dividing this concentration by the plasma EC_{50} of 0.15 μM in the rat DC-MES study results in a behavioral signs concentration (BSC) / plasma EC_{50} ratio of 473-fold. The same calculation was repeated for the established ASMs. The minimal plasma concentrations provoking behavioral signs for carbamazepine, phenytoin, and lacosamide were 110 μM , 11 μM , and 123 μM , respectively. Their plasma EC_{50} s were 30 μM , 4.5 μM , and 24.4 μM , respectively. **Figure 7E** shows BSC / Plasma EC_{50} ratios for carbamazepine (3.7-fold), phenytoin (2.4-fold), and lacosamide (5.0-fold). This data indicates that increasing $\text{Na}_v1.6$ selectivity can improve the tolerability of Na_v inhibitors in rodent-seizure models.

Discussion

Sodium channel inhibitors have long been, and remain, a mainstay of pharmacotherapy for epilepsy, as well as for pain and other neurologic, cardiac, and skeletal muscle disorders. The diverse range of indications and systems affected by these drugs is a testament to their critical biological role in cellular excitability. A fundamental challenge for these currently marketed sodium channel drugs is that none of them are selective amongst the nine sodium channel isoforms. As a result, drugs targeting the sodium channels of the brain for epilepsy can inhibit both excitatory and inhibitory neurons, limiting their ability to restore balanced neuronal firing.

Reducing $\text{Na}_v1.1$ current is proconvulsant due to the predominance of $\text{Na}_v1.1$ in inhibitory interneurons (Catterall et al., 2010; Claes et al., 2001; Escayg et al., 2000; Mistry et al., 2014; Yu et al., 2006), while the opposite is true for $\text{Na}_v1.2$ and $\text{Na}_v1.6$ currents (Ben-Shalom et al., 2017; Hawkins et al., 2011; Martin et al., 2007). $\text{Na}_v1.2$ and $\text{Na}_v1.6$ are more highly expressed in excitatory neurons (Catterall et al., 2010; Du et al., 2020; Encinas et al., 2020).

Additionally, these nonselective agents can block the channels associated with skeletal muscle ($\text{Na}_v1.4$), cardiac tissue ($\text{Na}_v1.5$), and peripheral neurons ($\text{Na}_v1.7$, $\text{Na}_v1.8$, $\text{Na}_v1.9$). Inhibiting these off-target channels can compromise muscular, cardiovascular, and sensory function. These risks are highlighted by the FDA's recent drug-safety communication for the nonselective Na_v inhibitor ASM lamotrigine. Lamotrigine has been linked to cardiac liabilities as a consequence of $\text{Na}_v1.5$ inhibition (FDA, 2021). Likewise, Na_v inhibitors intended as local anesthetics for trigeminal neuralgia or other pain syndromes and class I cardiac antiarrhythmic drugs are often dose limited by CNS adverse events like dizziness, sedation, and cognitive or motor impairment caused by inhibition of CNS Na_v channels (Caron and Libersa, 1997).

An obvious solution to this isoform selectivity challenge is to pursue a precision-medicine approach and create selective pharmacologic agents that preferentially target the sodium channels specific to the desired target tissue or cell type. This selective approach has been pursued for multiple channel isoforms - particularly for the peripheral Na_v s associated with pain ($\text{Na}_v1.3$, $\text{Na}_v1.7$, and $\text{Na}_v1.8$). This approach has proven challenging because the nine isoforms of sodium channels, $\text{Na}_v1.1$ - $\text{Na}_v1.9$, share a high degree of primary and tertiary structural similarity. Achieving selectivity with compounds that have tractable pharmaceutical properties has been particularly difficult.

Previous attempts to optimize Na_v inhibitors for epilepsy have focused on either drug properties or channel-state dependence. To our knowledge, this is the first description of acentrally penetrant, isoform-selective Na_v inhibitor for use in CNS indications, including epilepsy. NBI-921352 represents the first selective inhibitor of $\text{Na}_v1.6$ that is suitable for systemic oral administration.

The $\text{Na}_v1.6$ selective profile of NBI-921352 was designed to inhibit activity in excitatory neurons while sparing firing in the inhibitory interneurons where $\text{Na}_v1.1$ is preferentially expressed. We found that NBI-921352 did reduce firing in cortical excitatory pyramidal cells. In contrast, fast-firing inhibitory interneuron firing was not impaired and actually showed a trend toward increasing (although not statistically significant). The reason that interneuron action-potential firing might increase is unclear but could be a consequence of network effects that arise from interactions with other neurons synapsed onto the target neurons in the experiment. These data confirm that selective $\text{Na}_v1.6$ inhibitors can display differential inhibition of neurons in a manner that nonselective inhibitors, like carbamazepine, generally do not.

The distribution of $\text{Na}_v1.6$ to excitatory pyramidal neurons is not absolute, and $\text{Na}_v1.6$ expression has also been found in inhibitory interneurons. This is most well established for Purkinje neurons (Raman et al., 1997; Woodruff-Pak et al., 2006). Deletion of $\text{Na}_v1.6$ in Purkinje neurons in mice causes deficits in both cognition and motor control (Levin et al., 2006; Woodruff-Pak et al., 2006). $\text{Na}_v1.6$ is also highly expressed at the nodes of Ranvier of both central and peripheral neurons (Boiko et al., 2001; Caldwell et al., 2000; Herzog et al., 2003). We have found that selective inhibitors of $\text{Na}_v1.6$ can cause ataxia and motor symptoms when plasma and brain concentrations are very high (Figure 7). It is unclear whether these effects are due to concentrations exceeding those that retain high selectivity, or whether high occupancy of $\text{Na}_v1.6$ is directly responsible. In either case, our data would suggest that selective inhibition of $\text{Na}_v1.6$ provides a robust window between the level of inhibition required to reduce seizure induction and the levels that impair normal behavior.

SCN8A-RES patients most often carry de novo genetic variants. While some variants are known to be recurrent, many variants are represented by a single patient (Meisler, 2019). We therefore wanted to assure that NBI-921352 inhibition was not limited to wild-type $\text{Na}_v1.6$ channels. We tested nine distinct, patient-identified variants and found that 8 of them were inhibited by NBI-921352 at similar concentrations as wild-type channels (Figure 2). One variant, R1617Q, was found to be 6.8-fold less sensitive to inhibition than the wild-type channel. R1617Q has been identified in multiple SCN8A-DEE patients and is in the domain IV voltage-sensor domain (VSD4). NBI-921352 is an aryl sulfonamide with structural similarity to the $\text{Na}_v1.7$ targeted aryl sulfonamides where the binding site has been identified as the $\text{Na}_v1.7$ VSD4 (Ahuja et al., 2015; McCormack et al., 2013). It is likely that the R1617Q directly or allosterically impairs the tight association of NBI-921252 with $\text{Na}_v1.6$ due to its proximity to

the binding site. Despite the reduction in potency, NBI-921352 remains markedly more potent than existing Na_v inhibitor drugs on the R1617Q variant $\text{Na}_v1.6$ channel. This would suggest that while NBI-921352 may be an effective treatment for *SCN8A*-DEE patients carrying R1617Q variants, higher plasma levels of the compound could be required for efficacy in those patients.

Many *SCN8A*-RES-associated variants produce their GoF effects by disrupting or destabilizing the inactivation-gating machinery of $\text{Na}_v1.6$ channels. This can lead to pathological persistent or resurgent currents that contribute to neuronal hyperexcitability (*Pan and Cummins, 2020*).

Most known small molecule inhibitors of Na_v channels, except some marine toxins like tetrodotoxin, bind preferentially to inactivated gating states of the channels and stabilize the channels in inactivated, non-conductive conformations. This state dependence is manifested as a protocol dependence of the apparent drug potency. State dependence inhibition has been described in many ways. Use-dependent, frequency-dependent, resurgent current -selective, and persistent current-selective inhibition are all consequences of a preference for binding to inactivated channels. Stabilizing inactivated states of the channel reduces persistent and resurgent currents, and this feature has been suggested to contribute to the efficacy of many Na_v targeted ASMs including phenytoin, carbamazepine, oxcarbazepine, lacosamide, cannabidiol, and lamotrigine (*Wengert and Patel, 2021*). NBI-921352 is also highly state dependent, with a > 750 fold preference for inactivated channels vs. rested, closed-state channels (sometimes referred to as *peak current*). Forcing all $\text{Na}_v1.6$ channels into the closed state by applying voltages more hyperpolarized than physiological (−120 mV) results in very weak inhibition of the channels (*Figure 3*). Biasing the channels toward inactivated states by holding the membrane potential more positive in a protocol designed to monitor currents recovered from the inactivated state, resurgent current, or persistent current protocol all yielded potent inhibition. In physiologic conditions, channels are distributed among closed, open, and inactivated states, thus allowing equilibration of potent inhibition of the channel by NBI-921352.

Based on structural similarities and biophysical behavior, we believe that NBI-921352 binds to the domain IV voltage sensor domain (VSD4), much like GX-936 binds to the chimeric $\text{Na}_v1.7$ constructs in Ahuja et al. In this structure the VSD4 is captured in the up (activated) state. The down (rested) state of the voltage sensor is not available for high-affinity interaction with the compound. We expect that the high affinity binding events for NBI-921352 occur only when the VSD4 is in the up state, promoting inactivation. We believe this is the likely mechanism by which NBI-921352 traps channels in the inactivated state and reduces $\text{Na}_v1.6$ currents.

Increasing the selectivity of a Na_v inhibitor provides the expectation of an improved safety profile by reducing adverse events caused by off-target activity. An inherent risk of this approach is the potential loss of efficacy that could come from reduced polypharmacy. We have developed a potent, highly selective $\text{Na}_v1.6$ inhibitor in NBI-921352. Our studies with NBI-921352 indicate that a $\text{Na}_v1.6$ -specific compound can retain a robust ability to prevent seizures in rodent models at modest plasma and brain concentrations, consistent with the important role of $\text{Na}_v1.6$ in seizure pathways. Our data also suggests that this selectivity profile does improve the tolerability of NBI-921352 relative to commonly employed nonselective sodium channel ASMs in rodents. Whether these results will translate to humans is not yet established, but Phase I clinical trials have shown that NBI-921352 was well tolerated at plasma concentrations higher than were required for efficacy in the preclinical rodent studies described here. NBI-921352 is currently being developed for both *SCN8A*-DEE epilepsy and adult focal-onset seizures by *Neurocrine, 2019*. Phase II clinical trials will soon evaluate the efficacy of NBI-921352 in patients (*Neurocrine, 2021*). These clinical trials will provide the first evidence for whether the robust efficacy and tolerability demonstrated in rodents translates to human epilepsy patients.

Materials and methods

Key resources table

Reagent type (species) or resource	Designation	Source or reference	Identifiers	Additional information
Cell line (<i>H. sapiens</i>)	Expi293F	Thermo Fischer	cat# A14527	<i>SCN8A</i> mutant transient transfections
Cell line (<i>H. sapiens</i>)	FreeStyle 293 F	Thermo Fischer	cat# R710-07	Stable transfections

Continued on next page

Continued

Reagent type (species) or resource	Designation	Source or reference	Identifiers	Additional information
Strain, strain background (<i>M. musculus</i>)	C57BL/6 J male <i>Scn8a</i> ^{N1768D/+} (stock#400690) x C3HeB/FeJ female (strain#000658). Both Male and Female heterozygous <i>Scn8a</i> ^{N1768D/+} micewere tested	Licensed from Miriam Meisler, Univ. of Michigan. Wagnon et al., 2015		Colony maintained at The Jackson Laboratory
Strain, strain background (<i>M. musculus</i>)	CF-1, male	Charles River	Code: 023	
Strain, strain background (<i>R. norvegicus</i>)	Sprague Dawley, male	Envigo	Code: 002	
Chemical compound, drug	NBI-921352	US Patent #10246453 B2	Compound ID #101	Synthesized at Xenon Pharmaceuticals
Chemical compound, drug	Carbamazepine	Sigma-Aldrich	C4024	
Chemical compound, drug	Phenytoin	Sigma-Aldrich	D4505	
Chemical compound, drug	Lacosamide	Toronto Research Chemicals	L098500	
Gene (<i>H. sapiens</i>)	SCN1A	GenBank	NM_006920	
Gene (<i>H. sapiens</i>)	SCN2A	GenBank	NM_021007	
Gene (<i>H. sapiens</i>)	SCN3A	GenBank	NM_0069220	
Gene (<i>H. sapiens</i>)	SCN4A	GenBank	NM_000334	
Gene (<i>H. sapiens</i>)	SCN5A	GenBank	NM_198056	
Gene (<i>H. sapiens</i>)	SCN8A	GenBank	NM_014191	
Gene (<i>H. sapiens</i>)	SCN9A	GenBank	NM_002977	
Gene (<i>M. musculus</i>)	SCN1A	GenBank	NM_018733.2	
Gene (<i>M. musculus</i>)	SCN2A	GenBank	NP_001092768.1	
Gene (<i>M. musculus</i>)	SCN8A	GenBank	NM_001077499	
Gene (<i>H. sapiens</i>)	SCN1B	GenBank	NM_199037	
Gene (<i>H. sapiens</i>)	FGF13	GenBank	NM_033642	
Gene (<i>H. sapiens</i>)	CNTN1	GenBank	NM_001843	
Recombinant DNA reagent	pcDNA4/TO (vector)	Thermo Fischer	cat #V102020	Vector for SCNxA genes
Recombinant DNA reagent	pcDNA6/TR (regulatory vector for tetracycline repressor protein)	Thermo Fischer	cat#V102520	Vector to generate inducible FreeStyle 293 F and Expi293F
Recombinant DNA reagent	pcDNA3.1 (+) (vector)	Thermo Fischer	cat#V79020	Vector for SCN1B gene
Recombinant DNA reagent	pcDNA3.1/Hygro(+)	Thermo Fischer	cat# V87020	Vector for FGF13 and CNTN1 genes

Electrophysiological determination of potency and selectivity

Cell lines

Electrophysiology experiments were performed with HEK293 cells either stably transfected or transiently transfected. All of the cell lines tested negative for mycoplasma. The cell lines were authenticated by STR profiling at EuroFins Genomics. Stable cell lines were transfected with an expression vector containing the full-length cDNA coding for specific human and mouse sodium channel α -subunit, grown in culture media containing 10% fetal bovine serum, and 0.5 mg/mL Geneticin (G418) at 37 °C with 5% CO₂. The Na_v1.x stable cell lines and accessory constructs used correspond to the following GenBank accession numbers: Human Na_v1.1 (NM_006920); mouse Na_v1.1 (NM_018733.2); human Na_v1.2 (NM_021007); mouse Na_v1.2 (NP_001092768.1); human Na_v1.5 (NM_198056); human Na_v1.6 (NM_014191); mouse Na_v1.6 (NM_001077499); human Na_v1.7 (NM_002977); human Na_v1.4 (NM_000334); human Na_v1.3 (NM_0069220). The human Na_v β 1 subunit (NM_199037) was co-expressed in all cell lines. Human and mouse Na_v1.6 channels were also coexpressed with human FHF2B

(NM_033642) to increase functional expression. Human Na_v1.2 channels were also coexpressed with Contactin 1 (NM_001843) to increase functional expression.

For studies of mutant channels, cDNA plasmids in pcDNA4/TO Mammalian Expression Vector were transiently transfected into Expi293F cells stably expressing human FHF2b and human SCN1B subunit (polyclonal) background using ExpiFectamine 293 Transfection Kits (Gibco, Thermo Fisher Scientific CAT #: A14524). Induction was achieved using Tetracycline (Sigma Aldrich). Transfected cells were used in automated patch-clamp experiments 24 hours postinduction.

Na_v channel automated Qube 384 planar patch-clamp assays

NBI-921352 requires several seconds to equilibrate with activated channels, and this property of the compound must be taken into consideration in the design of state-dependent assay voltage-clamp protocols.

Data was collected using the Qube 384 (Sophion) automated voltage-clamp platform using single hole plates. To measure inactivated state inhibition, the membrane potential was maintained at a voltage where inactivation is complete. For each Na_v channel subtype, the V_h used to quantify compound inhibition were as follows: Na_v1.6 (-45 mV), Na_v1.1 (-45 mV), Na_v1.2 (-45 mV), Na_v1.3 (-45 mV), Na_v1.5 (-60 mV), Na_v1.7 (-60 mV), Na_v1.4 (-45 mV). The mutant channel hNa_v1.6^{N1768D} was found to have accelerated run-down compared with wild-type hNa_v1.6, so the holding potential was adjusted to -60 mV to provide sufficient signal window. The voltage was briefly repolarized to a negative voltage (-150 mV) for 20 ms for Na_v1.5, Na_v1.7, Na_v1.3, Na_v1.4 or for 60 ms for Na_v1.1, Na_v1.2, and Na_v1.6 to allow recovery from fast inactivation, followed by a test pulse to -20 or 0 mV for 10 ms to quantify the compound inhibition. The repolarization step allows compound-free channels to recover from fast inactivation, but compound-bound channels remain inhibited during the subsequent test step. For rested state 'Peak' current V_h was set to -120 mV. Appropriate filters for minimum seal resistance were applied (typically >500 MΩ membrane resistance), and series resistance was compensated at 100%. The pulse protocols were run at 1 Hz for hNa_v1.7, hNa_v1.5, hNa_v1.3, and hNa_v1.4 or 0.04 Hz for Na_v1.6, Na_v1.1 and Na_v1.2.

To construct concentration response curves, baseline currents were established after 20 min in vehicle (0.5% DMSO). Full inhibition response amplitudes were determined by adding tetrodotoxin (TTX, 300 nM) or tetracaine for Na_v1.5 (10 μM) to each well at the end of the experiment. Compounds were then exposed at a single concentration for 20 min. One-sixth of every experimental plate was dedicated to vehicle-only wells that enabled correction for nonspecific drift (i.e. rundown) of the signal in each experiment. For all channel subtypes, inhibition by the compound reached steady state within 20 min of incubation. The current inhibition values (I_(CPD)) were normalized to both the vehicle (I_(control)) and the full response defined by supramaximal TTX (I_(TTX)) or tetracaine (for Na_v1.5) addition responses according to Equation 1.

$$I_{norm(CPD)} = (I_{CPD} - I_{control}) / (I_{TTX} - I_{control}).$$

This normalized inhibition was then further normalized to the span of the assay to account for the run-down seen in cells exposed to vehicle alone for 20 min as follows:

Equation 2

$$I_{norm,span} = (I_{norm(CPD)} - I_{norm(VEH)}) / (1 - I_{norm(VEH)}), \text{ where :}$$

$I_{norm,span}$ = the current response normalized to within the span of the assay.

$I_{norm(CPD)}$ = the normalized response in the presence of compound.

$I_{norm(VEH)}$ = the normalized response in the absence of compound.

This normalization ensures that the data ranges were between 0 and 1, and there is no rundown in the plots. The normalized data from all cell recordings at a concentration were grouped together and plotted with GraphPad Prism 8, and IC₅₀ values were calculated for grouped data using the following version of the Hill equation:

Equation 3

$$Y = RD + (1 - RD) * [CPD] / (IC_{50} + [CPD]), \text{ where :}$$

Y = the fraction of sodium current blocked in the presence of the compound.

$[CPD]$ = the concentration of compound.

IC_{50} = the IC_{50} concentration.

RD = the 'rundown' of sodium current in vehicle alone, which is equal to 0 in this case, as the inhibition has already been normalized to the span.

The Hill slope was fixed to 1.

The 95% CI for the IC_{50} from the fitted curve to the mean data were reported unless otherwise noted.

To evaluate inhibition of $hNa_v1.6(N1768D)$ resurgent currents, synthetic $Na_v\beta4$ peptide (KKLITFILK-KTREKKKECLV) was added to the intracellular recording solution at 200 μ M and a dedicated protocol to elicit resurgent currents was employed (*Barbosa et al., 2015*). Cells were voltage clamped at ($V_h = -80$ mV) and subjected to a strong depolarization (+ 60 mV) for 20 ms. Following the strong depolarization, cells were partially repolarized to the voltage where resurgent current was maximal (-20 mV) for 50 ms, and resurgent current amplitude was measured. This resurgent current-specific waveform was repeated at 5 Hz for 100 s in vehicle, followed by 100 s in test compound, then 300 nM TTX. Fractional inhibition was calculated using the same normalization procedure as above.

Experiments were all performed at $27^\circ\text{C} \pm 2^\circ\text{C}$.

Automated patch-clamp recording solutions

The recording solutions for $Na_v1.1$, $Na_v1.2$, $Na_v1.3$, $Na_v1.4$ and $Na_v1.6$ cell line studies contained: Intracellular solution (ICS): 5 mM NaCl, 10 mM CsCl, 120 mM CsF, 0.1 mM $CaCl_2$, 2 mM $MgCl_2$, 10 mM HEPES (4-(2-hydroxyethyl)-1-piperazineethanesulfonic acid buffer), 10 mM EGTA (ethylene glycol tetraacetic acid); adjusted to pH 7.2 with CsOH. Extracellular solution (ECS): 140 mM NaCl, 5 mM KCl, 2 mM $CaCl_2$, 1 mM $MgCl_2$, 10 mM HEPES; adjusted to pH 7.4 with NaOH. Solutions with a reversed Na^+ gradient were used for $Na_v1.5$ and $Na_v1.7$ studies since they improved technical success. ICS: 120 mM NaF, 10 mM CsCl, 0.1 mM $CaCl_2$, 2 mM $MgCl_2$, 10 mM HEPES, 10 mM EGTA; adjusted to pH 7.2 with CsOH. ECS: 1 mM NaCl, 139 mM CholineCl, 5 mM KCl, 2 mM $CaCl_2$, 1 mM $MgCl_2$, 10 mM HEPES; adjusted to pH 7.4 with NaOH. Osmolarity in all ICS and ECS solutions was adjusted with glucose to 300 mOsm/kg and 310 mOsm/kg, respectively.

Current-clamp recording of cortical pyramidal neurons and inhibitory interneurons

Slice preparation

Parasagittal cortical brain slices were prepared from > P21 mice using standard procedures (adapted from Tai et al., PNAS 2014). Briefly, the mouse was deeply anaesthetized with isoflurane and decapitated. The brain was removed and placed into chilled artificial cerebrospinal fluid (aCSF) solution containing (in mM): 125 NaCl, 25 $NaHCO_3$, 2.5 KCl, 1.25 NaH_2PO_4 , 2 $CaCl_2$, 2 $MgCl_2$, 10 d-glucose, pH 7.3, osmolarity adjusted to ~306 mOsm using sucrose. All solutions were saturated with 95% O_2 and 5% CO_2 constantly perfused with 95% O_2 /5% CO_2 . Slices with a thickness of 400 μ m were prepared using a vibratome (Ted Pella, Inc). Following sectioning, the slices were placed in a holding chamber and incubated in a water bath at 34 $^\circ\text{C}$ for 15 min. The brain slices were removed from the water bath and held at room temperature for 60 min prior to recording.

Brain slice electrophysiology assay

All experiments involving rodent subjects were performed in accordance with the guidelines of the Canadian Council on Animal Care (CCAC). Following a 60-min incubation at room temperature, a brain slice was selected and placed on the stage of an upright microscope (SliceScope Pro 2000, Scientifica). The slice was constantly perfused with room temperature aCSF, containing 0.1% DMSO as a vehicle control, and oxygenated with 95% O_2 /5% CO_2 . The slice was visualized using brightfield microscopy, and a healthy neuron was selected from neocortical layer 5. Whole-cell configuration was achieved with a pipette (bath resistance 4–6 M Ω) containing internal solution. Stimulation was applied in current-clamp mode, and consisted of a series of 1000ms square pulses, beginning at -20 pA and increasing by +20 pA increments (3000ms between pulses).

Once the recordings in vehicle were completed, and while still holding the patch on the same neuron, the bath solution was changed from 0.1% DMSO in aCSF to 0.25 μ M NBI-921352 or 100 μ M Carbamazepine in aCSF. The slice was incubated in circulating compound for 10 min before repeating the series of square pulse stimulations. Working stock solutions were prepared in DMSO at a concentration of 20 mM.

All data analysis was done offline using ClampFit 10.7 (Molecular Devices). Data are presented as a mean \pm SEM. For each sweep, the number of evoked APs was counted, and plotted as a function of current injection (beginning with -20 pA). These generated 'input/output' (or 'F/I') curves demonstrating the relationship between stimulus and average AP frequency. Statistical significance was assessed using paired, two-way, student's t-test applied at each current injection level with significance considered $p < 0.05$.

Formulation and oral dosing of NBI-921352

Vehicle preparation

The vehicle for oral dosing solutions was 0.5% methyl cellulose and 0.2% Tween-80 in deionized (DI) water. DI water (0.8 L) was heated up to 70–80°C. Five grams of methyl cellulose was slowly added to heated DI water. The mixture was stirred until it formed a homogeneous milky suspension. The suspension was moved to a cold room and stirred overnight to get a clear solution. Two milliliters of Tween-80 was added to the clear solution and diluted up to 1 L with DI water. The vehicle solution was stored at 2–8°C.

Drug formulation

NBI-921352 was weighed into vials. An appropriate amount of vehicle was added to the NBI-921352 powder then mixed on a T18 ULTRA TURRAX homogenizer (IKA, Wilmington, NC) to create a uniform suspension at the desired concentration. The vials were then wrapped in aluminum foil to protect them from light and placed on a stir plate until the time of dosing. Carbamazepine and lacosamide were formulated in the same manner. Phenytoin was formulated in 0.9% physiological saline.

Dosing

NBI-921352, carbamazepine, and lacosamide were administered orally using a stainless-steel gavage needle at a dose volume of 10 ml/kg. Phenytoin was formulated in physiological saline and was administered intraperitoneally (i.p.) using a 25-gauge needle at a dose volume of 10 mL/kg. All compounds were administered 2 hr prior to electrical seizure induction for all seizure models employed in this study.

Bioanalytical assessment of plasma and brain concentrations

Sample collection:

Approximately 0.5 mL of blood was collected from each mouse at the end of the assay via cardiac puncture under deep anesthesia. The blood samples were collected in a syringe and transferred to tubes containing EDTA. Blood was stored at 4 °C until centrifuged within 30 min of collection. Plasma was harvested and placed on dry ice and stored in a freezer set to maintain a temperature of -70°C to -80°C until analysis. Brains were harvested immediately after blood collection and placed on dry ice prior to storage in a freezer set to maintain a temperature of -70°C to -80°C until analysis.

Plasma samples:

Extraction of plasma samples was carried out by protein precipitation using acetonitrile. Plasma samples (50 μ L) were mixed with 50 μ L of internal standard (IS) solution in water followed by addition of 10 μ L of concentrated ortho-phosphoric acid and 200 μ L of acetonitrile. Samples were vortexed for 30 seconds, centrifuged at 13,000 rpm for 20 min, decanted into a 96-well plate, and further centrifuged at 4000 rpm for 20 min. The samples were analyzed by UHPLC-ESI-MS/MS as described below.

Brain samples:

Prior to extraction, pre-weighed whole brains were homogenized in 1:1 acetonitrile/water (v/v) (4 mL per mouse brain) using an IKA T18 ULTRA-TURRAX Homogenizer at the setting of 4 for approximately

2 min. The homogenate was centrifuged at 13,000 rpm for 20 min and 50 μ L of the supernatant were treated exactly as described above for plasma samples. Fifty μ L of the brain homogenate were then treated exactly as the plasma samples described above.

Standards and quality control (QC) samples:

K₂EDTA Blank mouse plasma purchased from Valley Biomedical, California, USA was used to prepare standards and QC samples for plasma quantitation and as surrogates for brain homogenate quantitation. Calibration samples ranged from 2.34 ng/mL to 4800 ng/mL. QC samples concentration included 14 ng/mL (QC-L), 255 ng/mL (QC-M), and 3600 ng/mL (QC-H). Standards and QC samples were processed the same way as the sample extracts described above.

Analytical methods and statistics for plasma and tissue samples:

Samples were analyzed by UHPLC-ESI MS/MS using a TQ-5500 Sciex triple quadrupole mass spectrometer equipped with a Shimadzu Nexera UHPLC pump and auto-sampler system using an ACE C18 PFP, 2.50 \times 50 mm, 1.7 μ m particle size column and gradient elution consisting of solvent A (0.1% formic acid in water) and solvent B (0.1% formic acid in acetonitrile) starting at 20% B from 0 min to 0.4 min and then increased to 100% B from 0.4 min to 0.6 min. At 2.0 min, the mobile phase composition was switched back to 60% B for 1 min. The flow rate used throughout the experiment was 0.4 mL/min. The analyte, NBI-921352, and the IS were detected by electrospray in the positive ion mode using the following transitions: m/z 460/91 for NBI-921352 and m/z 503/341 m/z for the IS. The UHPLC-ESI MS/MS system was controlled by Analyst 1.6.

Sample concentrations were determined using a linear calibration function, weighted 1/X, generated by the regression of analyte to IS peak area ratios in the standard samples to their respective concentrations. Acceptance criteria for the analytical run required that the back calculated values of the standards and the QC samples fell within \pm 20% of their nominal values, except for the lowest standard or lower limit of quantitation (LLOQ), for which the acceptance criterion was \pm 25%. At least 6 out of 12 standard points had to show back-calculated values within \pm 20% of their nominal concentrations for the calibration to be accepted. At least three QC samples, one at each level, had to show back-calculated values within \pm 20% of their nominal concentrations for the whole sample batch to be valid.

Animals

After delivery, animals were allowed sufficient time to acclimate prior to testing (~1 week). All animals were housed in plastic cages in rooms with controlled humidity, ventilation, and lighting (12 hr/12 hr light–dark cycle). All animal procedures were performed using protocols approved by Xenon Animal Care Committee and the Canadian Council on Animal Care.

Scn8a^{N1768D/+} mice:

Xenon Pharmaceuticals Inc licensed the mouse with the missense mutation p.Asn1768Asp (N1768D) in the neuronal sodium channel Na_v1.6, characterized and developed by Dr. M Meisler (University of Michigan, MI, USA). The *Scn8a*^{N1768D} knock-in allele was generated by TALEN targeting of (C57BL/6JXSJL) F2 eggs at the University of Michigan Transgenic Animal Model Core. The line was propagated by backcrossing N1768D/+ heterozygotes to C57BL/6 J wild-type mice (The Jackson Laboratory, Bar Harbor, ME). Male N1768D/+ heterozygotes on a C57BL/6 J background were subsequently backcrossed to C3HeB/FeJ female mice. All the experiments were performed using animals following at least seven such backcrosses. Experiments were performed using (B6 \times C3 He) F7 (F7. N1768D/+) offspring aged 35–42 days.

WT mice:

Adult male CF-1 WT albino mice 26–35 g were obtained from Charles River, Senneville, Quebec, Canada. All the assays were carried out in mice 9–12 weeks of age.

Sprague-Dawley rats:

Adult male Sprague-Dawley albino rats weighing 150–200 g were obtained from Envigo, Livermore, CA, USA. All the assays were carried out in rats aged 5–6 weeks.

The modified 6 Hz psychomotor seizure assay

Scn8a^{N1768D/+} heterozygous mice were tested at 5 weeks of age (p35). The modified 6 Hz seizure assay in *Scn8a*^{N1768D/+} heterozygous mice was adapted from the traditional 6 Hz assay psychomotor seizure assay to provide a measure of in vivo on target (Na_v1.6 mediated) efficacy (Barton et al., 2001). The modified assay used a low frequency (6 Hz) but long-duration stimulation (3 s) to induce seizures. We identified 12 mA and a 0.3-ms pulse interval as a suitable current for testing in *Scn8a*^{N1768D/+} mice, since it differentiated mutant and wild-type (WT) mice. An electroshock (6 Hz, 12 mA) was delivered for 3 s (at 0.3-ms pulse interval) by corneal electrodes (Electro Convulsive Therapy Unit 57,800 from Ugo Basile). Immediately prior to the electroshock, the animals' eyes were anesthetized with a drop of Alcaine (0.5% proparacaine hydrochloride). Upon corneal stimulation, WT mice experienced mild seizure behaviors such as facial clonus, forelimb clonus, Straub tail, rearing, and falling, but did not experience a generalized tonic-clonic seizure (GTC) with hindlimb extension. *Scn8a*^{N1768D/+} animals, however, in addition to mild seizure behaviors, experienced a GTC with hindlimb extension. The modified assay showed a clear differentiation of seizure behavior between WT and *Scn8a*^{N1768D/+} mice. *Scn8a*^{N1768D/+} mice exhibited GTC with hindlimb extension but not WT mice.

For the single-dose and repeated-dose efficacy experiments, *Scn8a*^{N1768D/+} animals were dosed PO with vehicle or NBI-921352 two hours before the administration of the electric stimulation. An animal was considered protected in the assay upon prevention of GTC with hindlimb extension and was then scored '0'. An animal displaying GTC with hindlimb extension was considered not protected and is then scored '1'. The experimenter scoring the seizure behavior was blinded to the treatment.

DC-Maximal electroshock seizure assay in rodents

The maximal electroshock seizure (MES) assay has been extensively used in the search for anticonvulsant substances (Löscher et al., 1991; Piredda et al., 1985; White et al., 1995). The MES assay is sensitive to nonselective NaV inhibitors. It is considered a model for generalized tonic-clonic (GTC) seizures and provides an assessment of seizure spread. Briefly, an electroshock of direct current (DC) was delivered by corneal electrodes (Electro Convulsive Therapy Unit 57,800 from Ugo Basile). The parameters of stimulation were different between mice and rats. In CF1 mice aged 9–12 weeks, a direct current of 50 mA (60 Hz) was delivered for 0.2 s (pulse width of 0.5ms), whereas in Sprague Dawley (SD) rats aged 5–6 weeks, a direct current of 150 mA (60 Hz) was delivered for 0.3 s (pulse width of 0.5ms). Immediately prior to the electroshock, the animals' eyes were anesthetized with a drop of Alcaine (0.5% proparacaine hydrochloride). Upon corneal stimulation, naive animals experienced a generalized tonic-clonic seizure (GTC) with hindlimb extension.

For the efficacy experiments, single dose and repeated dose, animals were dosed PO with vehicle or NBI-921352 2 hr before the administration of the electric stimulation. An animal was considered protected in the assay in the absence of a GTC with hindlimb extension and is then scored '0'. An animal displaying GTC with hindlimb extension was considered not protected and is then scored '1'. The experimenter scoring the seizure behavior was blinded to the treatment.

Blinding of in vivo efficacy experiments

On each testing day, individual treatment groups were assigned a random label (e.g. A, B, C, etc.) by the technical staff administering the compound. To ensure blinding, the technical staff member performing drug administration differed from the person performing the test. Therefore, the experimenter conducting testing was blinded to treatment group (e.g. drug or vehicle treatment, dose, and time point).

Randomization of in vivo efficacy experiments

Randomization of animals into various treatment groups occurred on a per-animal (e.g. rather than a per-cage) basis. Therefore, each animal was randomly assigned to a treatment group, and all animals tested in each experiment had an equal chance of assignment to any treatment group. Prior to each study, a randomization sequence was obtained (<https://www.graphpad.com/quickcalcs/>).

Observation of potential adverse behavior for Figure 7

Animals were observed by the scientist(s) responsible for dosing for the first 30 min after dosing for and again at the time of assay (2 hr post dose) for signs of abnormal behavior. Abnormal behavioral

signs were noted for all compounds – tremor, ataxia and hypoactivity – when plasma concentrations were sufficiently high. The lowest concentration at which such behavioral signs were noted in any of the animals tested is illustrated by the dotted line in **Figure 7**. Animals that exhibited abnormal behavior were not assessed in efficacy assays.

Data processing and analysis

All statistics were calculated using GraphPad Prism version eight software. All fraction seizing data plotted by dose groups is expressed as an absolute fraction of all tested animals that seized (number of animals that seized / the number of animals tested). Racine score data is reported in **Figure 5—figure supplements 1 and 2**, and in **Figure 6—figure supplements 1 and 2**, and 3. Racine score data are plotted by dose groups and are expressed as mean \pm SEM. Between-group differences were compared to vehicle response and were analyzed using a Kruskal-Wallis test followed by Dunn's multiple comparisons test (fraction seizing data) or ordinary one-way ANOVA followed by Dunnett's multiple comparison test (Racine score data). Statistical significance was reached at values of $p < 0.05$. More detailed results of the statistical analysis, with p values, is presented in the figure supplements and legends.

Acknowledgements

We thank Dr. Fiona Scott, PhD of Neurocrine Biosciences for thoughtful discussions and commentary on this manuscript. We thank Ian Mortimer of Xenon Pharmaceuticals for strategic discussions. We thank Dr. Miriam Meisler, PhD for making *Scn8a*^{N1768D/+} mice available. We thank the SCN8A-RES patients, families and patient advocates for detailed discussions regarding the clinical presentation of SCN8A mutations and unmet medical needs in their community.

Additional information

Competing interests

JP Johnson, Thilo Focken, Kuldip Khakh, Celine Dube, Samuel J Goodchild, Jean-Christophe Andrez, Girish Bankar, Kristen Burford, Elaine Chang, Sultan Chowdhury, Richard Dean, Gina de Boer, Shannon Decker, Christoph Dehnhardt, Mandy Feng, Wei Gong, Michael Grimwood, Abid Hasan, Angela Hussainkhel, Qi Jia, Stephanie Lee, Jenny Li, Sophia Lin, Andrea Lindgren, Verner Lofstrand, Janette Mezeyova, Rostam Namdari, Karen Nelkenbrecher, Noah Gregory Shuart, Luis Sojo, Shaoyi Sun, Matthew Taron, Matthew Waldbrook, Diana Weeratunge, Steven Wesolowski, Aaron Williams, Michael Wilson, Zhiwei Xie, Rhena Yoo, Clint Young, Alla Zenova, Wei Zhang, Alison J Cutts, Robin P Sherrington, Simon N Pimstone, Raymond Winqvist, Charles J Cohen, James R Empfield: is employed by Xenon Pharmaceuticals, Inc and may hold equity in Xenon Pharmaceuticals, Inc. Parisa Karimi Tari, David Bogucki: was previously employed by Xenon Pharmaceuticals, Inc and may hold equity in Xenon Pharmaceuticals, Inc.

Funding

Funder	Grant reference number	Author
Xenon Pharmaceuticals, Inc		JP Johnson Thilo Focken Kuldip Khakh Parisa Karimi Tari Celine Dube Samuel J Goodchild Jean-Christophe Andrez Girish Bankar David Bogucki Kristen Burford Elaine Chang Sultan Chowdhury Richard Dean Gina de Boer Shannon Decker Christoph Dehnhardt Mandy Feng Wei Gong Michael Grimwood Abid Hasan Angela Hussainkhel Qi Jia Stephanie Lee Jenny Li Sophia Lin Andrea Lindgren Verner Lofstrand Janette Mezeyova Rostam Namdari Karen Nelkenbrecher Noah Gregory Shuart Luis Sojo Shaoyi Sun Matthew Taron Matthew Waldbrook Diana Weeratunge Steven Wesolowski Aaron Williams Michael Wilson Zhiwei Xie Rhena Yoo Clint Young Alla Zenova Wei Zhang Alison J Cutts Robin P Sherrington Simon N Pimstone Raymond Winquist Charles J Cohen James R Empfield

All of this work was funded by Xenon Pharmaceuticals, and all of the authors are, or were previously, employees of Xenon Pharmaceuticals.

Author contributions

JP Johnson, Conceptualization, Data curation, Formal analysis, Methodology, Project administration, Supervision, Visualization, Writing – original draft, Writing – review and editing; Thilo Focken, Conceptualization, Data curation, Formal analysis, Supervision, Writing – review and editing; Kuldip Khakh, Steven Wesolowski, Aaron Williams, Data curation, Formal analysis, Methodology, Supervision, Writing – review and editing; Parisa Karimi Tari, Celine Dube, Samuel J Goodchild, Jean-Christophe Andrez, Girish Bankar, David Bogucki, Kristen Burford, Elaine Chang, Sultan Chowdhury, Richard Dean, Christoph Dehnhardt, Mandy Feng, Wei Gong, Michael Grimwood, Abid Hasan, Angela Hussainkhel, Qi Jia, Stephanie Lee, Jenny Li, Sophia Lin, Verner Lofstrand, Janette Mezeyova, Rostam Namdari, Karen Nelkenbrecher, Noah Gregory Shuart, Luis Sojo, Shaoyi Sun, Matthew Taron, Matthew Waldbrook, Diana Weeratunge, Michael Wilson, Zhiwei Xie, Rhena Yoo, Clint Young, Alla Zenova, Wei Zhang, Data curation, Formal analysis, Methodology, Writing – review and editing; Gina de Boer, Andrea Lindgren,

Data curation, Formal analysis, Writing – review and editing; Shannon Decker, Data curation, Formal analysis, Methodology, Project administration, Writing – review and editing; Alison J Cutts, Data curation, Formal analysis, Project administration, Writing – original draft, Writing – review and editing; Robin P Sherrington, Conceptualization, Funding acquisition, Project administration, Writing – review and editing; Simon N Pimstone, Funding acquisition, Project administration, Supervision, Writing – review and editing; Raymond Winkquist, Data curation, Formal analysis, Project administration, Writing – review and editing; Charles J Cohen, James R Empfield, Conceptualization, Funding acquisition, Project administration, Supervision, Writing – review and editing

Author ORCIDs

JP Johnson  <http://orcid.org/0000-0002-5762-5138>

Alison J Cutts  <http://orcid.org/0000-0002-4986-573X>

Ethics

All animal research was overseen by the Xenon Animal Care Committee and the Canadian Animal Care Council (CACC) according to the recommendations of the CACC (<https://ccac.ca/>).

Decision letter and Author response

Decision letter <https://doi.org/10.7554/eLife.72468.sa1>

Author response <https://doi.org/10.7554/eLife.72468.sa2>

Additional files

Supplementary files

- Transparent reporting form

Data availability

All the numerical data used to generate the figures in contained in the excel data source file included in the submission.

References

- Ahern CA, Payandeh J, Bosmans F, Chanda B. 2016. The hitchhiker's guide to the voltage-gated sodium channel galaxy. *The Journal of General Physiology* **147**:1–24. DOI: <https://doi.org/10.1085/jgp.201511492>, PMID: [26712848](https://pubmed.ncbi.nlm.nih.gov/26712848/)
- Ahuja S, Mukund S, Deng L, Khakh K, Chang E, Ho H, Shriver S, Young C, Lin S, Johnson JP Jr, Wu P, Li J, Coons M, Tam C, Brillantes B, Sampang H, Mortara K, Bowman KK, Clark KR, Estevez A, et al. 2015. Structural basis of Nav1.7 inhibition by an isoform-selective small-molecule antagonist. *Science (New York, N.Y.)* **350**:aac5464. DOI: <https://doi.org/10.1126/science.aac5464>, PMID: [26680203](https://pubmed.ncbi.nlm.nih.gov/26680203/)
- Barbosa C, Tan Z-Y, Wang R, Xie W, Strong JA, Patel RR, Vasko MR, Zhang J-M, Cummins TR. 2015. Navβ4 regulates fast resurgent sodium currents and excitability in sensory neurons. *Molecular Pain* **11**:60. DOI: <https://doi.org/10.1186/s12990-015-0063-9>, PMID: [26408173](https://pubmed.ncbi.nlm.nih.gov/26408173/)
- Barton ME, Klein BD, Wolf HH, White HS. 2001. Pharmacological characterization of the 6 Hz psychomotor seizure model of partial epilepsy. *Epilepsy Research* **47**:217–227. DOI: [https://doi.org/10.1016/s0920-1211\(01\)00302-3](https://doi.org/10.1016/s0920-1211(01)00302-3), PMID: [11738929](https://pubmed.ncbi.nlm.nih.gov/11738929/)
- Bean BP, Cohen CJ, Tsien RW. 1983. Lidocaine block of cardiac sodium channels. *The Journal of General Physiology* **81**:613–642. DOI: <https://doi.org/10.1085/jgp.81.5.613>, PMID: [6306139](https://pubmed.ncbi.nlm.nih.gov/6306139/)
- Beatch GN, Rostam;L, Gordon A, Ernesto. 2020. Pharmacokinetics, Food Effect, and Relative Bioavailability of Two Formulations of NBI-921352/XEN901 (Novel Nav1.6-Selective Sodium Channel Blocker) [In Healthy Adults: Pediatric Granules and Adult Tablets. Paper presented at the American Epilepsy Society Annual Meeting]. https://www.xenon-pharma.com/wp-content/uploads/2020/12/AES20_XEN901food_FINAL.pdf [Accessed December 7, 2020].
- Ben-Shalom R, Keeshen CM, Berrios KN, An JY, Sanders SJ, Bender KJ. 2017. Opposing Effects on Nav 1.2 Function Underlie Differences Between SCN2A Variants Observed in Individuals With Autism Spectrum Disorder or Infantile Seizures. *Biological Psychiatry* **82**:224–232. DOI: <https://doi.org/10.1016/j.biopsych.2017.01.009>, PMID: [28256214](https://pubmed.ncbi.nlm.nih.gov/28256214/)
- Boerma RS, Braun KP, van den Broek MPH, van de Broek MPH, van Berkestijn FMC, Swinkels ME, Hagebeuk EO, Lindhout D, van Kempen M, Boon M, Nicolai J, de Kovel CG, Brilstra EH, Koeleman BPC. 2016. Remarkable Phenytoin Sensitivity in 4 Children with SCN8A-related Epilepsy: A Molecular Neuropharmacological Approach. *Neurotherapeutics* **13**:192–197. DOI: <https://doi.org/10.1007/s13311-015-0372-8>, PMID: [26252990](https://pubmed.ncbi.nlm.nih.gov/26252990/)
- Boiko T, Rasband MN, Levinson SR, Caldwell JH, Mandel G, Trimmer JS, Matthews G. 2001. Compact myelin dictates the differential targeting of two sodium channel isoforms in the same axon. *Neuron* **30**:91–104. DOI: [https://doi.org/10.1016/s0896-6273\(01\)00265-3](https://doi.org/10.1016/s0896-6273(01)00265-3), PMID: [11343647](https://pubmed.ncbi.nlm.nih.gov/11343647/)

- Braakman HM**, Verhoeven JS, Erasmus CE, Haaxma CA, Willemsen MH, Schelhaas HJ. 2017. Phenytoin as a last-resort treatment in SCN8A encephalopathy. *Epilepsia Open* **2**:343–344. DOI: <https://doi.org/10.1002/epi4.12059>, PMID: 29588963
- Burgess DL**, Kohrman DC, Galt J, Plummer NW, Jones JM, Spear B, Meisler MH. 1995. Mutation of a new sodium channel gene, *Scn8a*, in the mouse mutant “motor endplate disease.” *Nature Genetics* **10**:461–465. DOI: <https://doi.org/10.1038/ng0895-461>, PMID: 7670495
- Caldwell JH**, Schaller KL, Lasher RS, Peles E, Levinson SR. 2000. Sodium channel Na(v)1.6 is localized at nodes of ranvier, dendrites, and synapses. *PNAS* **97**:5616–5620. DOI: <https://doi.org/10.1073/pnas.090034797>, PMID: 10779552
- Caron J**, Libersa C. 1997. Adverse effects of class I antiarrhythmic drugs. *Drug Safety* **17**:8–36. DOI: <https://doi.org/10.2165/00002018-199717010-00002>, PMID: 9258628
- Catterall WA**, Kalume F, Oakley JC. 2010. NaV1.1 channels and epilepsy. *The Journal of Physiology* **588**:1849–1859. DOI: <https://doi.org/10.1113/jphysiol.2010.187484>, PMID: 20194124
- Chen Q**, Kirsch GE, Zhang D, Brugada R, Brugada J, Brugada P, Potenza D, Moya A, Borggrefe M, Breithardt G, Ortiz-Lopez R, Wang Z, Antzelevitch C, O’Brien RE, Schulze-Bahr E, Keating MT, Towbin JA, Wang Q. 1998. Genetic basis and molecular mechanism for idiopathic ventricular fibrillation. *Nature* **392**:293–296. DOI: <https://doi.org/10.1038/32675>, PMID: 9521325
- Claes L**, Del-Favero J, Ceulemans B, Lagae L, Van Broeckhoven C, De Jonghe P. 2001. De novo mutations in the sodium-channel gene *SCN1A* cause severe myoclonic epilepsy of infancy. *American Journal of Human Genetics* **68**:1327–1332. DOI: <https://doi.org/10.1086/320609>, PMID: 11359211
- Colombo E**, Franceschetti S, Avanzini G, Mantegazza M. 2013. Phenytoin inhibits the persistent sodium current in neocortical neurons by modifying its inactivation properties. *PLOS ONE* **8**:e55329. DOI: <https://doi.org/10.1371/journal.pone.0055329>, PMID: 23383157
- Courtney KR**, Kendig JJ, Cohen EN. 1978. The rates of interaction of local anesthetics with sodium channels in nerve. *The Journal of Pharmacology and Experimental Therapeutics* **207**:594–604 PMID: 712641.,
- Du J**, Simmons S, Brunklaus A, Adiconis X, Hession CC, Fu Z, Li Y, Shema R, Møller RS, Barak B, Feng G, Meisler M, Sanders S, Lerche H, Campbell AJ, McCarroll S, Levin JZ, Lal D. 2020. Differential excitatory vs inhibitory SCN expression at single cell level regulates brain sodium channel function in neurodevelopmental disorders. *European Journal of Paediatric Neurology* **24**:129–133. DOI: <https://doi.org/10.1016/j.ejpn.2019.12.019>, PMID: 31928904
- Encinas AC**, Watkins JC, Longoria IA, Johnson JP, Hammer MF. 2020. Variable patterns of mutation density among NaV1.1, NaV1.2 and NaV1.6 point to channel-specific functional differences associated with childhood epilepsy. *PLOS ONE* **15**:e0238121. DOI: <https://doi.org/10.1371/journal.pone.0238121>, PMID: 32845893
- Escayg A**, MacDonald BT, Meisler MH, Baulac S, Huberfeld G, An-Gourfinkel I, Brice A, LeGuern E, Moulard B, Chaigne D, Buresi C, Malafosse A. 2000. Mutations of *SCN1A*, encoding a neuronal sodium channel, in two families with GEFS+2. *Nature Genetics* **24**:343–345. DOI: <https://doi.org/10.1038/74159>, PMID: 10742094
- FDA**. 2021. Drug Safety Communication: Studies show increased risk of heart rhythm problems with seizure and mental health medicine lamotrigine (Lamictal) in patients with heart disease. <https://www.fda.gov/drugs/drug-safety-and-availability/studies-show-increased-risk-heart-rhythm-problems-seizure-and-mental-health-medicine-lamotrigine> [Accessed March 31, 2021].
- Focken T**, Burford K, Grimwood ME, Zenova A, Andrez JC, Gong W, Wilson M, Taron M, Decker S, Lofstrand V, Chowdhury S, Shuart N, Lin S, Goodchild SJ, Young C, Soriano M, Tari PK, Waldbrook M, Nelkenbrecher K, Kwan R, et al. 2019. Identification of CNS-Penetrant Aryl Sulfonamides as Isoform-Selective Nav 1.6 Inhibitors with Efficacy in Mouse Models of Epilepsy. *Journal of Medicinal Chemistry* **62**:9618–9641. DOI: <https://doi.org/10.1021/acs.jmedchem.9b01032>, PMID: 31525968
- Gardella E**, Møller RS. 2019. Phenotypic and genetic spectrum of SCN8A-related disorders, treatment options, and outcomes. *Epilepsia* **60 Suppl 3**:S77–S85. DOI: <https://doi.org/10.1111/epi.16319>, PMID: 31904124
- Gennaro E**, Veggiotti P, Malacarne M, Madia F, Cecconi M, Cardinali S, Cassetti A, Cecconi I, Bertini E, Bianchi A, Gobbi G, Zara F. 2003. Familial severe myoclonic epilepsy of infancy: truncation of Nav1.1 and genetic heterogeneity *Epileptic Disorders* **5**:21–25 PMID: 12773292.,
- Hammer MF**, Wagnon JL, Mefford HC, Meisler MH. 2016. GeneReviews((R)). Seattle , WA.
- Hawkins NA**, Martin MS, Frankel WN, Kearney JA, Escayg A. 2011. Neuronal voltage-gated ion channels are genetic modifiers of generalized epilepsy with febrile seizures plus. *Neurobiology of Disease* **41**:655–660. DOI: <https://doi.org/10.1016/j.nbd.2010.11.016>, PMID: 21156207
- Herzog RI**, Cummins TR, Ghassemi F, Dib-Hajj SD, Waxman SG. 2003. Distinct repriming and closed-state inactivation kinetics of Nav1.6 and Nav1.7 sodium channels in mouse spinal sensory neurons. *The Journal of Physiology* **551**:741–750. DOI: <https://doi.org/10.1113/jphysiol.2003.047357>, PMID: 12843211
- Inglis GAS**, Wong JC, Butler KM, Thelin JT, Mistretta OC, Wu X, Lin X, English AW, Escayg A. 2020. Mutations in the *Scn8a* DIIS4 voltage sensor reveal new distinctions among hypomorphic and null Na_v1.6 sodium channels. *Genes, Brain, and Behavior* **19**:e12612. DOI: <https://doi.org/10.1111/gbb.12612>, PMID: 31605437
- Johannesen KM**, Gardella E, Encinas AC, Lehesjoki A-E, Linnankivi T, Petersen MB, Lund ICB, Blichfeldt S, Miranda MJ, Pal DK, Lascelles K, Procopis P, Orsini A, Bonuccelli A, Giacomini T, Helbig I, Fenger CD, Sisodiya SM, Hernandez-Hernandez L, Krithika S, et al. 2019. The spectrum of intermediate SCN8A-related epilepsy. *Epilepsia* **60**:830–844. DOI: <https://doi.org/10.1111/epi.14705>, PMID: 30968951
- Levin SI**, Khaliq ZM, Aman TK, Grieco TM, Kearney JA, Raman IM, Meisler MH. 2006. Impaired motor function in mice with cell-specific knockout of sodium channel *Scn8a* (Nav1.6) in cerebellar purkinje neurons and granule cells. *Journal of Neurophysiology* **96**:785–793. DOI: <https://doi.org/10.1152/jn.01193.2005>, PMID: 16687615

- Liu Y, Schubert J, Sonnenberg L, Helbig KL, Høe-Hansen CE, Koko M, Rannap M, Lauxmann S, Huq M, Schneider MC, Johannesen KM, Kurlmann G, Gardella E, Becker F, Weber YG, Benda J, Möller RS, Lerche H. 2019. Neuronal mechanisms of mutations in SCN8A causing epilepsy or intellectual disability. *Brain* **142**:376–390. DOI: <https://doi.org/10.1093/brain/awy326>, PMID: 30615093
- Löschner W, Fassbender CP, Nolting B. 1991. The role of technical, biological and pharmacological factors in the laboratory evaluation of anticonvulsant drugs. II. Maximal electroshock seizure models. *Epilepsy Research* **8**:79–94. DOI: [https://doi.org/10.1016/0920-1211\(91\)90075-q](https://doi.org/10.1016/0920-1211(91)90075-q), PMID: 2065646
- Martin MS, Tang B, Papale LA, Yu FH, Catterall WA, Escayg A. 2007. The voltage-gated sodium channel Scn8a is a genetic modifier of severe myoclonic epilepsy of infancy. *Human Molecular Genetics* **16**:2892–2899. DOI: <https://doi.org/10.1093/hmg/ddm248>, PMID: 17881658
- Mason ER, Wu F, Patel RR, Xiao Y, Cannon SC, Cummins TR. 2019. Resurgent and Gating Pore Currents Induced by De Novo SCN2A Epilepsy Mutations. *ENEURO* **6**:ENEURO.0141-19.2019. DOI: <https://doi.org/10.1523/ENEURO.0141-19.2019>, PMID: 31558572
- McCormack K, Santos S, Chapman ML, Krafte DS, Marron BE, West CW, Krambis MJ, Antonio BM, Zellmer SG, Printzenhoff D, Padilla KM, Lin Z, Wagoner PK, Swain NA, Stuppel PA, de Groot M, Butt RP, Castle NA. 2013. Voltage sensor interaction site for selective small molecule inhibitors of voltage-gated sodium channels. *PNAS* **110**:E2724–E2732. DOI: <https://doi.org/10.1073/pnas.1220844110>, PMID: 23818614
- Meisler MH. 2019. SCN8A encephalopathy: Mechanisms and models. *Epilepsia* **60 Suppl 3**:S86–S91. DOI: <https://doi.org/10.1111/epi.14703>, PMID: 31904118
- Mistry AM, Thompson CH, Miller AR, Vanoye CG, George AL, Kearney JA. 2014. Strain- and age-dependent hippocampal neuron sodium currents correlate with epilepsy severity in Dravet syndrome mice. *Neurobiology of Disease* **65**:1–11. DOI: <https://doi.org/10.1016/j.nbd.2014.01.006>, PMID: 24434335
- Neurocrine. 2019. Neurocrine Biosciences and Xenon Pharmaceuticals Announce Agreement to Develop First-in-Class Treatments for Epilepsy. <https://neurocrine.gcs-web.com/news-releases/news-release-details/neurocrine-biosciences-and-xenon-pharmaceuticals-announce> [Accessed December 2, 2019].
- Neurocrine. 2021. Study to Evaluate NBI-921352 as Adjunctive Therapy in Subjects With SCN8A Developmental and Epileptic Encephalopathy Syndrome (SCN8A-DEE) [ClinicalTrials.gov Retrieved from]. <https://www.clinicaltrials.gov/ct2/show/NCT04873869?term=NCT04873869&draw=2&rank=1> [Accessed May 5, 2021].
- Pan Y, Cummins TR. 2020. Distinct functional alterations in SCN8A epilepsy mutant channels. *The Journal of Physiology* **598**:381–401. DOI: <https://doi.org/10.1113/JP278952>, PMID: 31715021
- Piredda SG, Woodhead JH, Swinyard EA. 1985. Effect of stimulus intensity on the profile of anticonvulsant activity of phenytoin, ethosuximide and valproate. *The Journal of Pharmacology and Experimental Therapeutics* **232**:741–745 PMID: 3919174.,
- Potet F, Egecioglu DE, Burridge PW, George AL. 2020. GS-967 and Eleclazine Block Sodium Channels in Human Induced Pluripotent Stem Cell-Derived Cardiomyocytes. *Molecular Pharmacology* **98**:540–547. DOI: <https://doi.org/10.1124/molpharm.120.000048>, PMID: 32938719
- Ptáček LJ, George AL Jr, Griggs RC, Tawil R, Kallen RG, Barchi RL, Robertson M, Leppert MF. 1991. Identification of a mutation in the gene causing hyperkalemic periodic paralysis. *Cell* **67**:1021–1027. DOI: [https://doi.org/10.1016/0092-8674\(91\)90374-8](https://doi.org/10.1016/0092-8674(91)90374-8), PMID: 1659948
- Raman IM, Bean BP. 1997. Resurgent sodium current and action potential formation in dissociated cerebellar Purkinje neurons. *The Journal of Neuroscience* **17**:4517–4526 PMID: 9169512.,
- Raman IM, Sprunger LK, Meisler MH, Bean BP. 1997. Altered subthreshold sodium currents and disrupted firing patterns in Purkinje neurons of Scn8a mutant mice. *Neuron* **19**:881–891. DOI: [https://doi.org/10.1016/s0896-6273\(00\)80969-1](https://doi.org/10.1016/s0896-6273(00)80969-1), PMID: 9354334
- Rojas CV, Wang JZ, Schwartz LS, Hoffman EP, Powell BR, Brown RH. 1991. A Met-to-Val mutation in the skeletal muscle Na⁺ channel alpha-subunit in hyperkalemic periodic paralysis. *Nature* **354**:387–389. DOI: <https://doi.org/10.1038/354387a0>, PMID: 1659668
- Royeck M, Horstmann MT, Remy S, Reitze M, Yaari Y, Beck H. 2008. Role of axonal NaV1.6 sodium channels in action potential initiation of CA1 pyramidal neurons. *Journal of Neurophysiology* **100**:2361–2380. DOI: <https://doi.org/10.1152/jn.90332.2008>, PMID: 18650312
- Strichartz G. 1976. Molecular mechanisms of nerve block by local anesthetics. *Anesthesiology* **45**:421–441. DOI: <https://doi.org/10.1097/00000542-197610000-00012>, PMID: 9844
- Tidball AM, Lopez-Santiago LF, Yuan Y, Glenn TW, Margolis JL, Clayton Walker J, Kilbane EG, Miller CA, Martina Bebin E, Scott Perry M, Isom LL, Parent JM. 2020. Variant-specific changes in persistent or resurgent sodium current in SCN8A-related epilepsy patient-derived neurons. *Brain* **143**:3025–3040. DOI: <https://doi.org/10.1093/brain/awaa247>, PMID: 32968789
- Veeramah KR, O'Brien JE, Meisler MH, Cheng X, Dib-Hajj SD, Waxman SG, Talwar D, Girirajan S, Eichler EE, Restifo LL, Erickson RP, Hammer MF. 2012. De novo pathogenic SCN8A mutation identified by whole-genome sequencing of a family quartet affected by infantile epileptic encephalopathy and SUDEP. *American Journal of Human Genetics* **90**:502–510. DOI: <https://doi.org/10.1016/j.ajhg.2012.01.006>, PMID: 22365152
- Wagnon JL, Korn MJ, Parent R, Tarpey TA, Jones JM, Hammer MF, Murphy GG, Parent JM, Meisler MH. 2015. Convulsive seizures and SUDEP in a mouse model of SCN8A epileptic encephalopathy. *Human Molecular Genetics* **24**:506–515. DOI: <https://doi.org/10.1093/hmg/ddu470>, PMID: 25227913
- Wagnon JL, Meisler MH. 2015. Recurrent and Non-Recurrent Mutations of SCN8A in Epileptic Encephalopathy. *Frontiers in Neurology* **6**:104. DOI: <https://doi.org/10.3389/fneur.2015.00104>, PMID: 26029160

- Walia KS**, Khan EA, Ko DH, Raza SS, Khan YN. 2004. Side effects of antiepileptics--a review. *Pain Practice* **4**:194–203. DOI: <https://doi.org/10.1111/j.1533-2500.2004.04304.x>, PMID: 17173601
- Wengert ER**, Tronhjem CE, Wagnon JL, Johannesen KM, Petit H, Krey I, Saga AU, Panchal PS, Strohm SM, Lange J, Kamphausen SB, Rubboli G, Lemke JR, Gardella E, Patel MK, Meisler MH, Møller RS. 2019. Biallelic inherited SCN8A variants, a rare cause of SCN8A-related developmental and epileptic encephalopathy. *Epilepsia* **60**:2277–2285. DOI: <https://doi.org/10.1111/epi.16371>, PMID: 31625145
- Wengert ER**, Patel MK. 2021. The Role of the Persistent Sodium Current in Epilepsy. *Epilepsy Currents* **21**:40–47. DOI: <https://doi.org/10.1177/1535759720973978>, PMID: 33236643
- White HS**, Johnson M, Wolf HH, Kupferberg HJ. 1995. The early identification of anticonvulsant activity: role of the maximal electroshock and subcutaneous pentylentetrazol seizure models. *Italian Journal of Neurological Sciences* **16**:73–77. DOI: <https://doi.org/10.1007/BF02229077>, PMID: 7642355
- Woodruff-Pak DS**, Green JT, Levin SI, Meisler MH. 2006. Inactivation of sodium channel Scn8A (Na-sub(v)1.6) in Purkinje neurons impairs learning in Morris water maze and delay but not trace eyeblink classical conditioning. *Behavioral Neuroscience* **120**:229–240. DOI: <https://doi.org/10.1037/0735-7044.120.2.229>, PMID: 16719687
- Yu FH**, Mantegazza M, Westenbroek RE, Robbins CA, Kalume F, Burton KA, Spain WJ, McKnight GS, Scheuer T, Catterall WA. 2006. Reduced sodium current in GABAergic interneurons in a mouse model of severe myoclonic epilepsy in infancy. *Nature Neuroscience* **9**:1142–1149. DOI: <https://doi.org/10.1038/nn1754>, PMID: 16921370
- Zaman T**, Abou Tayoun A, Goldberg EM. 2019. A single-center SCN8A-related epilepsy cohort: clinical, genetic, and physiologic characterization. *Annals of Clinical and Translational Neurology* **6**:1445–1455. DOI: <https://doi.org/10.1002/acn3.50839>, PMID: 31402610